Ligand Mobility and Solution Structures of the Metallocenium Ion Pairs [$Me_2C(Cp)(fluorenyl)MCH_2SiMe_3^+\cdots X^-$] (M = Zr, Hf; X = $MeB(C_6F_5)_3$, $B(C_6F_5)_4$)

Carlos Alonso-Moreno,[†,‡] Simon J. Lancaster,[†] Joseph A. Wright,[†] David L. Hughes,[†] Cristiano Zuccaccia,[§] Andrea Correa,[⊥] Alceo Macchioni,*[,§] Luigi Cavallo,*[,⊥] and Manfred Bochmann*[,†]

Wolfson Materials and Catalysis Centre, School of Chemical Sciences and Pharmacy, University of East Anglia, Norwich NR4 7TJ, U.K., Dipartimento di Chimica, Università di Perugia, I-06123 Perugia, Italy, and Dipartimento di Chimica, Università di Salerno, I-84084 Fisciano, Italy

Received May 28, 2008

The mixed-alkyl metallocene complexes (IPCF)M(Me)(CH_2SiMe_3) (M = Zr, Hf; IPCF = $Me_2C(C_5H_4)(C_{13}H_8)$) were synthesized by the reaction of (IPCF)M(Me)Cl (M = Zr, Hf) with Me_3SiCH_2MgCl. The crystal structures of (IPCF)Zr(CH_2SiMe_3)$_2$, (IPCF)$HfMe_2$, and (IPCF)Zr(Me)Cl were determined by X-ray diffraction. The kinetics of site epimerization of the ion pairs (IPCF)M(CH_2SiMe_3)(μ-Me)$B(C_6F_5)_3$ and [(IPCF)$MCH_2SiMe_3^+\cdots B(C_6F_5)_4^-$] (M = Zr, Hf) were studied by variable-temperature NMR spectroscopy, while the solution ground-state structures of the ion pairs [$LZrCH_2SiMe_3^+\cdots B(C_6F_5)_4^-$] (L = SBI, IPCF; SBI = *rac*-$Me_2Si(Ind)_2$) were probed experimentally by $^{19}F,^1H$ HOESY NMR spectroscopy and theoretically by DFT and molecular dynamics calculations. They reveal differences in the strength of anion interactions between the SBI and IPCF systems which may be significant for their catalytic activity. The tetraarylborate salts are stabilized by agostic interactions to ligand Si−Me moieties, with Hf > Zr. The exchange rates of both the $MeB(C_6F_5)_3^-$ and the $B(C_6F_5)_4^-$ compounds increase with increasing ion pair concentration. This acceleration is also seen on addition of excess $[Ph_3C][B(C_6F_5)_4]$. Pulsed-field gradient spin−echo (PGSE) NMR measurements indicated that both [(IPCF)$ZrCH_2SiMe_3^+\cdots B(C_6F_5)_4^-$] and [(SBI)$ZrCH_2SiMe_3^+\cdots B(C_6F_5)_4^-$] were present mainly as ion quadruples in toluene-d_8/1,2-$F_2C_6H_4$ (8/2 in volume) at millimolar concentrations and, notably, their aggregation increased to a similar extent with the addition of an excess of $[Ph_3C][B(C_6F_5)_4]$. The results demonstrate the formation of mixed-ion aggregates of the type $\{[(L)MR^+\cdots X^-][CPh_3^+\cdots X^-]_n\}$. However, whereas the site epimerization rates k_{ex} of the system (SBI)ZrMe(CH_2SiMe_3)/$[Ph_3C][B(C_6F_5)_4]$ continue to increase linearly with the total ion concentration, for (IPCF)ZrMe(CH_2SiMe_3)/$[Ph_3C][B(C_6F_5)_4]$ mixtures k_{ex} reaches a plateau at ca. 400 s^{-1} (at 20 °C). Measurement of site epimerization rates as a function of ion pair concentration $[(A^+)_x(B^+)_{1-x}X^-]$ therefore provides evidence for the existence of a rate-limiting barrier in the IPCF system, while it is absent in others.

Introduction

As a number of kinetic and mechanistic investigations have shown recently,[1−8] the polymerization of alkenes is catalyzed by group 4 metallocenium ion pairs [$L_2M-R^+\cdots X^-$] (M = Ti, Zr, Hf), or quite possibly by the more fluxional ion quadruples,[3−5] and follows a number of reaction steps: (i) the displacement of the counteranion from its equilibrium position in an associative interchange (I_a) mechanism,[2b] (ii) dissymmetric monomer coordination,[6] (iii) migratory chain transfer to the β-carbon of the coordinated monomer, and (iv) reassociation of the anion into an equilibrium position that mirrors the starting point of the insertion process (Scheme 1).[2b,5,7c] In the polymerization of small monomers such as ethene or propene, the

* To whom correspondence should be addressed. E-mail: m.bochmann@uea.ac.uk (M.B.).
† University of East Anglia.
‡ Present address: Departamento de Química Inorgánica, Orgánica y Bioquímica, Universidad de Castilla-La Mancha, E-13071-Ciudad Real, Spain.
§ Università di Perugia.
⊥ Università di Salerno.

(1) Reviews: (a) Bochmann, M. *J. Organomet. Chem.* **2004**, *689*, 3982. (b) Erker, G. *Acc. Chem. Res.* **2001**, *34*, 309. (c) Chen, E. Y.-X.; Marks, T. J. *Chem. Rev.* **2000**, *100*, 1391. (d) Resconi, L.; Cavallo, L.; Fait, A.; Piemontesi, F. *Chem. Rev.* **2000**, *100*, 1253. (e) Bochmann, M. *J. Chem. Soc., Dalton Trans.* **1996**, 255. (f) Brintzinger, H. H.; Fischer, D.; Mülhaupt, R.; Rieger, B.; Waymouth, R. *Angew. Chem., Int. Ed. Engl.* **1995**, *34*, 1143. (g) Jordan, R. F. *Adv. Organomet. Chem.* **1991**, *32*, 325.

(2) (a) Song, F.; Cannon, R. D.; Bochmann, M. *J. Am. Chem. Soc.* **2003**, *125*, 7641. (b) Song, F.; Hannant, M. D.; Cannon, R. D.; Bochmann, M. *Macromol. Symp.* **2004**, *213*, 173. (c) Bochmann, M.; Song, F.; Rodriguez, A.; Cannon, R. D. *PMSE Prepr.* **2002**, *87*, 36. (d) Rodriguez-Delgado, A.; Hannant, M. D.; Lancaster, S. J.; Bochmann, M. *Macromol. Chem. Phys.* **2004**, *205*, 334. (e) Bochmann, M.; Cannon, R. D.; Song, F. *Kinet. Catal.* **2006**, *47*, 160. (f) Zhou, J.; Lancaster, S. J.; Walker, D. A.; Beck, S.; Thornton-Pett, M.; Bochmann, M. *J. Am. Chem. Soc.* **2001**, *123*, 223.

(3) (a) Beck, S.; Geyer, A.; Brintzinger, H. H. *Chem. Commun.* **1999**, 2477. (b) Beck, S.; Lieber, S.; Schaper, F.; Geyer, A.; Brintzinger, H. H. *J. Am. Chem. Soc.* **2001**, *123*, 1483. (c) Babushkin, D. E.; Brintzinger, H. H. *J. Am. Chem. Soc.* **2002**, *124*, 12869. (d) Wieser, U.; Babushkin, D.; Brintzinger, H. H. *Organometallics* **2002**, *21*, 920.

(4) (a) Abramo, G. P.; Li, L.; Marks, T. J. *J. Am. Chem. Soc.* **2002**, *124*, 13966. (b) Stahl, N. G.; Zuccaccia, C.; Jensen, T. R.; Marks, T. J. *J. Am. Chem. Soc.* **2003**, *125*, 5256. (c) Zuccaccia, C.; Stahl, N. G.; Macchioni, A.; Chen, M. C.; Roberts, J. A.; Marks, T. J. *J. Am. Chem. Soc.* **2004**, *126*, 1448.

(5) Song, F.; Lancaster, S. J.; Cannon, R. D.; Schormann, M.; Humphrey, S. M.; Zuccacia, C.; Macchioni, A.; Bochmann, M. *Organometallics* **2005**, *24*, 1315.

10.1021/om800486p CCC: $40.75
Publication on Web 09/30/2008

Scheme 1

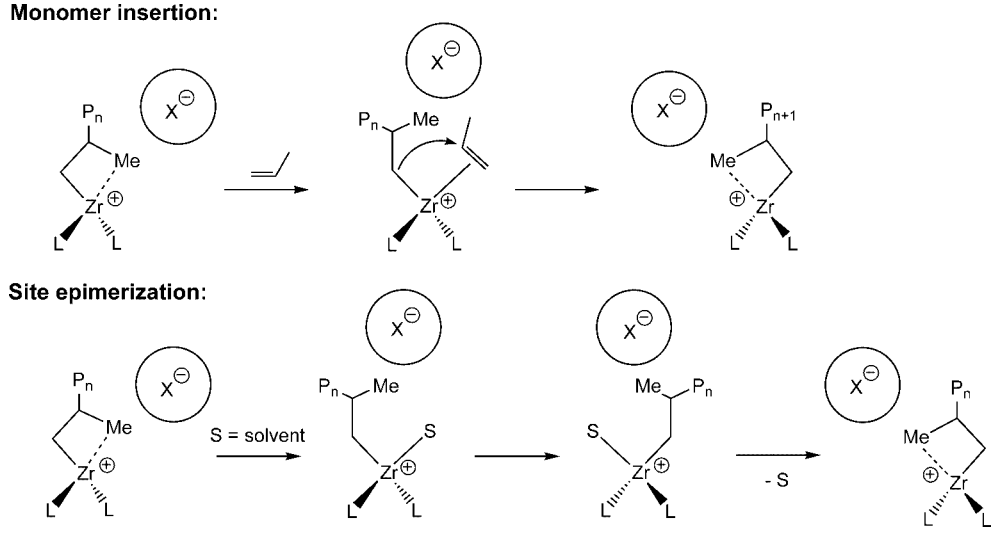

first step (anion displacement) tends to be rate determining, since it increases the cation−anion separation and hence costs electrostatic energy.[9]

A process closely related to the monomer insertion sequence is site epimerization,[8] which interchanges the positions of the alkyl ligand and the anion; this operation is often referred to as ion pair symmetrization or "anion exchange" (characterized by the first-order rate constant k_{ex}). This process involves reaction steps i and iv. Here, too, the rate-limiting step is anion displacement, this time not by the monomer but by the solvent. Site epimerization is slower than monomer insertion for most catalysts,[10] including those under discussion here, since anion substitution by the solvent is less facile than by monomer. Nevertheless, in cases where step i contributes significantly to the rate-limiting step, the rates of both site epimerization and monomer insertion should follow similar trends, since the same limiting factors will be operative.

The polymerization catalysts $[(SBI)Zr-R^+\cdots B(C_6F_5)_4^-]$[11] and $[(IPCF)Zr-R^+\cdots B(C_6F_5)_4^-]$[12] are quite similar in steric demand, since in both cases the ligand framework is made up of two five-membered rings annulated by two six-membered rings (SBI = *rac*-Me_2Si(1-indenyl)$_2$; IPCF = $Me_2C(C_5H_4)$(9-fluorenyl)). They differ, however, very significantly in their propene polymerization productivities, and they differ also in their response to increased concentrations of trityl salt: whereas under closely comparable conditions the system (SBI)$ZrCl_2$/TIBA/$[Ph_3C][B(C_6F_5)_4]$ shows a productivity increase from ca. 80×10^6 to almost 200×10^6 g of PP (mol of Zr)$^{-1}$ h^{-1} bar^{-1} on raising the CPh_3^+:Zr ratio from 1:1 to 3:1 (at 25 °C/1 bar and constant [Zr]; TIBA = $AlBu^i_3$), the system (IPCF)$ZrCl_2$/TIBA/$[Ph_3C][B(C_6F_5)_4]$ gives no such activator response and exhibits approximately constant and comparatively low productivities of ca. 25×10^6 g of PP (mol of Zr)$^{-1}$ h^{-1} bar^{-1}, irrespective of the trityl concentration (Figure 1).[13]

At the time of our original report,[13] we were not in a position to put forward a satisfactory explanation for the presence or absence of this "trityl effect" in metallocene catalysts. Several scenarios might be envisaged to explain the lack of such an effect in IPCF catalysts; for example: (i) the anion might be more tightly bonded than in SBI analogues, (ii) since ligand fluxionality has been shown to be enhanced in ion aggregates,[3−5] a reduced tendency to form such aggregates might negatively affect catalytic performance, (iii) chain growth might involve a late transition state that is little influenced by anion mobility (see for example ref 9), or (iv) the IPCF ion pair might be unstable. We wondered whether a measurement of the site epimerization rates k_{ex} might provide at least some of the answers. We also wished to explore to what extent such site exchange rates might be regarded as a guide to catalyst activity. It is noted in this context that Marks et al. reported the effect

(6) (a) Horton, A. D.; Orpen, A. G. *Organometallics* **1992**, *11*, 8. (b) Wu, Z.; Jordan, R. F.; Petersen, J. L. *J. Am. Chem. Soc.* **1995**, *117*, 5867. (c) Carpentier, J. F.; Wu, Z.; Lee, C. W.; Strömberg, S.; Christopher, J. N.; Jordan, R. F. *J. Am. Chem. Soc.* **2000**, *122*, 7750. (d) Casey, C. P.; Carpenetti, D. W. *Organometallics* **2000**, *19*, 3970. (e) Casey, C. P.; Carpenetti, D. W.; Sakurai, H. *Organometallics* **2001**, *20*, 4262. (f) Brandow, C. G.; Mendiratta, A.; Bercaw, J. E. *Organometallics* **2001**, *20*, 4253.

(7) (a) Lui, Z.; Somsook, E.; White, C. B.; Rosaaen, A.; Landis, C. R. *J. Am. Chem. Soc.* **2001**, *123*, 11193. (b) Landis, C. R.; Rosaaen, K. A.; Uddin, J. *J. Am. Chem. Soc.* **2002**, *124*, 12062. (c) Landis, C. R.; Rosaeen, K. A.; Sillars, D. R. *J. Am. Chem. Soc.* **2003**, *125*, 1710. (d) Sillars, D. R.; Landis, C. R. *J. Am. Chem. Soc.* **2003**, *125*, 9894. (e) Landis, C. R.; Sillars, D. R.; Batterton, J. M. *J. Am. Chem. Soc.* **2004**, *126*, 8890. (f) Busico, V.; Cipullo, R.; Romanelli, V.; Ronca, S.; Togrou, M. *J. Am. Chem. Soc.* **2005**, *127*, 1608. (g) Busico, V.; Cipullo, R.; Esposito, V. *Macromol. Rapid Commun.* **1999**, *20*, 116. (h) Lin, S.; Tagge, C. D.; Waymouth, R. M.; Nele, M.; Collins, S.; Pinto, J. C. *J. Am. Chem. Soc.* **2000**, *122*, 11275.

(8) (a) Beck, S.; Prosenc, M. H.; Brintzinger, H. H.; Goretzki, R.; Herfert, N.; Fink, G. *J. Mol. Catal. A: Chem.* **1996**, *111*, 67. (b) Deck, P. A.; Marks, T. J. *J. Am. Chem. Soc.* **1995**, *117*, 6128. (c) Deck, P. A.; Beswick, C. L.; Marks, T. J. *J. Am. Chem. Soc.* **1998**, *120*, 1772. (d) Luo, L.; Marks, T. J. *Top. Catal.* **1999**, *7*, 97. (e) Siedle, A. R.; Newmark, R. A. *J. Organomet. Chem.* **1995**, *497*, 119. (f) Siedle, A. R.; Hanggi, B.; Newmark, R. A.; Mann, K. R.; Wilson, T. *Macromol. Symp.* **1995**, *89*, 299. (g) Brandow, C. G.; Mendiratta, A.; Bercaw, J. E. *Organometallics* **2001**, *20*, 4253. (h) Bercaw, J. E.; Miller, S. A. *Organometallics* **2006**, *25*, 3576. (i) Nele, M.; Mohammed, M.; Xin, S. X.; Collins, S.; Dias, M. L.; Pinto, J. C. *Macromolecules* **2001**, *34*, 3830.

(9) Song, F.; Cannon, R. D.; Bochmann, M. *Chem. Commum.* **2004**, 542.

(10) In only a few cases, such as for the C_1-symmetric catalysts (Cp-Z-Ind)ZrR(X) (Z = CMe_2, $SiMe_2$; X = MeMAO, $MeB(C_6F_5)_3$, $B(C_6F_5)_4$), has site epimerization been shown to be significantly faster than chain propagation: Mohammed, M.; Nele, M.; Al-Humydi, A.; Xin, S.; Stapleton, R. A.; Collins, S. *J. Am. Chem. Soc.* **2003**, *125*, 7930.

(11) Bochmann, M.; Lancaster, S. J.; Hursthouse, M. B.; Malik, K. M. A. *Organometallics* **1994**, *13*, 2235.

(12) (a) Ewen, J. A.; Elder, M. J.; Jones, R. L.; Haspelagh, L.; Atwood, J. L.; Bott, S. G.; Robinson, K. *Makromol. Chem. Macromol. Symp.* **1991**, *48/49*, 253. (b) Ewen, J. A.; Elder, M. J. *Makromol. Chem., Macromol. Symp.* **1993**, *66*, 179. (c) Bochmann, M.; Lancaster, S. J. *Organometallics* **1993**, *12*, 633. (d) Bochmann, M.; Lancaster, S. J. *Macromol. Rapid Commun.* **1993**, *14*, 807.

(13) Song, F.; Cannon, R. D.; Lancaster, S. J.; Bochmann, M. *J. Mol. Catal.* **2004**, *218*, 21.

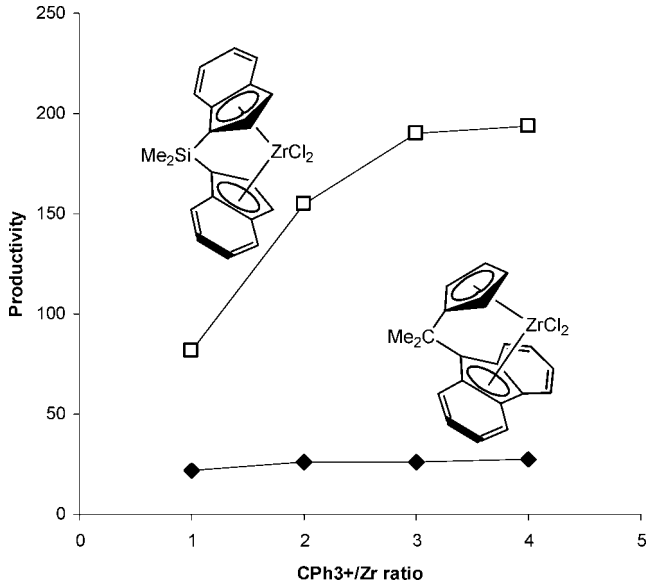

Figure 1. Propene polymerization activity and response to the CPh_3^+:Zr ratio of (SBI)$ZrCl_2$ (□) and (IPCF)$ZrCl_2$ precatalysts (◆) (1 bar of propene, 100 mL of toluene, $[Ph_3C][B(C_6F_5)_4]$, Al^iBu_3 10^{-3} mol L^{-1}, 25 °C). The unit of productivity is 10^6 g of PP (mol of Zr)$^{-1}$ h^{-1} bar^{-1} (data from ref 13).

of more strongly coordinating anions on the activity and stereoselectivity of IPCF-based catalysts.[14]

As we have argued previously,[5,9] the CH_2SiMe_3 alkyl ligand represents a more realistic model for the growing polymeryl chain than the frequently used methyl ligand,[8] a view supported by recent calculations.[15] We report here the synthesis and site epimerization rates of $[(IPCF)Zr{-}R^+\cdots X^-]$ ion pairs (R = CH_2SiMe_3; X = $MeB(C_6F_5)_3$, $B(C_6F_5)_4$) in comparison with the analogous $[(SBI)Zr{-}R^+\cdots B(C_6F_5)_4^-]$ system. In a preliminary communication we have shown recently the first evidence for the formation of mixed-ion aggregates $[\{LZrR^+\}_n\{CPh_3^+\}_m\{X^-\}_{(n+m)}]$ in the presence of excess trityl borate salts and its influence on site epimerization rates.[16]

Results and Discussion

Synthesis of Metal Dialkyl Complexes. The reaction of (IPCF)$ZrCl_2$[17] with 1 equiv of Me_3SiCH_2MgCl is not selective for the monoalkylation product; the reaction proceeds instead to the highly soluble dialkyl species (IPCF)$Zr(CH_2SiMe_3)_2$ **1**. The hafnium dichloride (IPCF)$HfCl_2$ is even less soluble, and we therefore chose to prepare the alkyl complex in a one-pot reaction from the ligand. The crude dichloride complex reacted only very slowly with Me_3SiCH_2MgCl at room temperature to give a mixture of mono- and dialkylated complexes. However, heating to 80 °C overnight gave quantitative conversion (by ^{1}H NMR) to the dialkyl compound (IPCF)$Hf(CH_2SiMe_3)_2$ (**2**) (Scheme 2). The M−CH_2 hydrogen atoms are diastereotopic, with chemical shift differences of $\Delta\delta$ = 1.92 and 0.79 ppm for **1** and **2**, respectively.

The dimethyl compounds (IPCF)MMe_2 (M = Zr (**3**), Hf (**4**))[18] were synthesized in one-pot reactions from the fluorenyl ligand and MCl_4, followed by the addition of 2 equiv of MeMgCl to the crude dichloride complexes, to give **3** and **4** in good yields (Scheme 2).

Whereas attempted alkyl abstraction or ligand exchange reactions with **1** or **2** either did not proceed or did not lead to the desired products, one of the methyl ligands of **3** and **4** can be exchanged for chloride by treatment with an equimolar amount of Ph_3CCl (Scheme 3),[19] to give the corresponding monomethyl complexes (IPCF)M(Me)Cl (M = Zr (**5**), Hf (**6**)). The reaction requires 2 h at 50 °C for the zirconium derivative and 16 h at 70 °C for the hafnium analogue. The ^{1}H NMR spectra show the lowering of symmetry in these chiral complexes, with four multiplets being observed for the Cp group and two singlets for the methyl groups of the CMe_2 bridge.

The reaction of (IPCF)Zr(Me)Cl (**5**) with 1 equiv of Me_3SiCH_2MgCl in toluene gives cleanly the mixed-alkyl complex (IPCF)Zr(Me)(CH_2SiMe_3) (**7**) (Scheme 3). Preparation of the hafnium analogue (IPCF)Hf(Me)(CH_2SiMe_3) (**8**) is less facile, and complex **6** must be treated with Me_3SiCH_2MgCl overnight at 70 °C to ensure complete conversion. Related mixed-alkyl complexes bearing C_2-symmetric[5,9] and 1,2-$C_5H_3Me_2$ ligands[20] have been reported. The ^{1}H NMR spectra of **7** and **8** confirm the C_1 symmetry. The hydrogen atoms of the metal-bound CH_2 groups are diastereotopic, with one hydrogen experiencing a significant high-field chemical shift.

The structure of **1** was confirmed by X-ray diffraction; only in the orientation of the CH_2SiMe_3 ligands is there significant deviation from mirror symmetry (Figure 2). In the crystal, the alkyl ligands differ in rotation about the Zr−C bonds. The bond C(5)−H(5b) points directly into the center of the C(12,13,16−19) ring (H···C distances in the range 2.77−3.00 Å), but on C(6), the hydrogen atoms are aligned so that H(6b) has contact with C(14,20,21) of the second six-membered ring, and H(6a) interacts with C(34,35) of the C_5H_4 group. The bridge carbon atom C(1) is displaced by 0.386(14) and 0.253(13) Å from the mean planes of the two five-membered rings, illustrating the strain in this ligand in its bonding about the Zr atom. The angle subtended by the centroids of the two rings at the Zr atom is 116.5°.

The C_1-symmetric complex **5** was also characterized by crystal structure analysis and adopts the expected geometry (Figure 3). The methyl and chloride ligands are disordered over the two meridional coordination sites on the ligand, in an approximately 2:1 ratio. The zirconium atom is found closer to the Cp ring (Zr−Ct_{Cp} = 2.174 Å) than to the fluorenyl ring (Zr−Ct_{Flu} = 2.268 Å). The angle subtended by the centroids at the metal is 117.9° in this case. For the structural characterization of the essentially isostructural Hf dimethyl complex **4**, see the Supporting Information.

Formation of Inner-Sphere Ion Pairs. Treatment of **7** and **8** with $B(C_6F_5)_3$ leads to methyl abstraction to give the inner-sphere ion pair[21] complexes (IPCF)M(CH_2SiMe_3)(μ-Me)B-$(C_6F_5)_3$ (M = Zr (**9**), Hf (**10**), respectively) (Scheme 3). Abstraction is completely selective for the methyl group within ^{1}H NMR detection limits.[22]

Both **9** and **10** are fluxional in solution, as shown by variable-temperature NMR spectroscopy (Figure 4). The bridge CMe_2 signals are resolved as two singlets at room temperature which

(14) (a) Chen, M. C.; Marks, T. J. *J. Am. Chem. Soc.* **2001**, *123*, 11803. (b) Chen, M. C.; Roberts, J. A. S.; Marks, T. J. *J. Am. Chem. Soc.* **2004**, *126*, 4605. (c) Chen, M. C.; Roberts, J. A. S.; Marks, T. J. *Organometallics* **2004**, *23*, 932.

(15) Ducère, J. M.; Cavallo, L. *Organometallics* **2006**, *25*, 1431.

(16) Alonso-Moreno, C.; Lancaster, S. J.; Zuccaccia, C.; Macchioni, A.; Bochmann, M. *J. Am. Chem. Soc.* **2007**, *129*, 9282.

(17) Ewen, J. A.; Lonew, R. L.; Razavi, A. *J. Am. Chem. Soc.* **1988**, *110*, 6255.

(18) (a) Razavi, A.; Ferrara, J. *J. Organomet. Chem.* **1992**, *435*, 299. (b) Razavi, A.; Thewalt, U. *J. Organomet. Chem.* **1993**, *445*, 111.

(19) Hawrelak, E. J.; Deck, P. A. *Organometallics* **2004**, *23*, 9.

(20) Beswick, C. L.; Marks, T. J. *J. Am. Chem. Soc.* **2000**, *122*, 10358.

Scheme 2

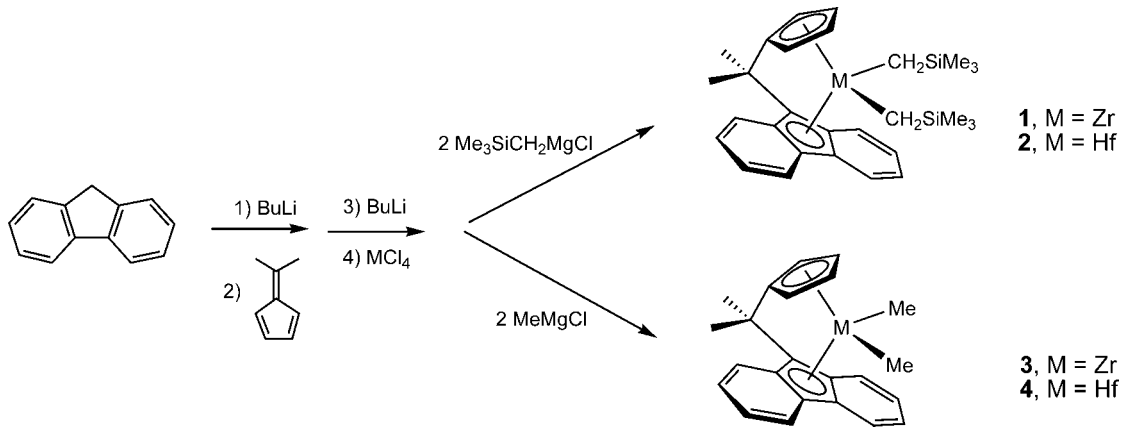

Scheme 3

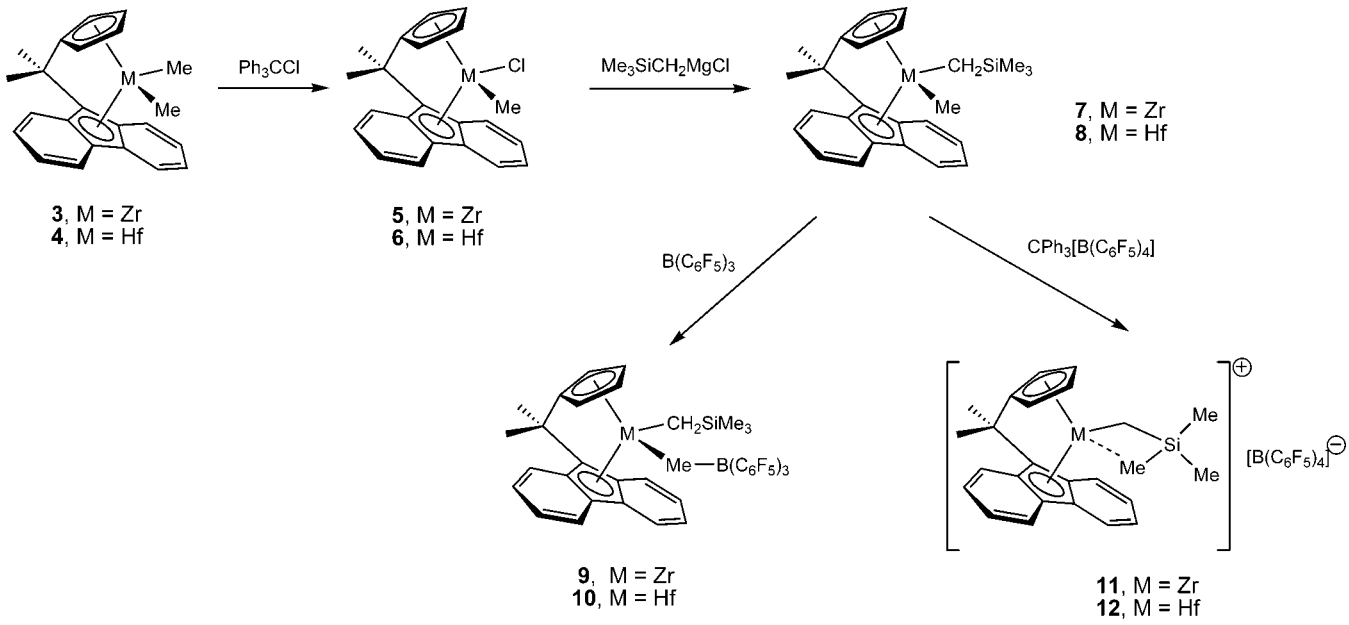

coalesce at 60 °C for **9** and at 65 °C for **10**: evidence of slow site exchange of the CH_2SiMe_3 and $MeB(C_6F_5)_3$ ligands. As in the neutral mixed-alkyl complexes **7** and **8**, the M−CH_2 moieties of **9** and **10** are diastereotopic and appear as two doublets with a chemical shift difference of $\Delta\delta = 1.11$ for **9** and $\Delta\delta = 1.38$ for **10** at 20 °C. The μ-Me proton resonance appears as a broad signal in the region typical of this chemical environment (δ −0.59 for **9** and −0.44 for **10**).[8,22]

Formation of Outer-Sphere Ion Pairs. The reaction of group 4 zirconocene dimethyls with $[Ph_3C][B(C_6F_5)_4]$ to give catalytically active cationic metal alkyl species has been shown to proceed in two steps: the fast formation of a methyl-bridged binuclear cation[8a,23] followed by a much slower reaction with further CPh_3^+ to give the mononuclear ion pair $[L_2Zr\text{-}Me^+\cdots B(C_6F_5)_4^-]$.[2f] In contrast, on reacting $[Ph_3C][B(C_6F_5)_4]$ with the mixed-alkyl complexes **7** and **8** (Zr:B = 1:1) in aromatic solvents at room temperature, the formation of methyl-bridged binuclear products could not be observed, and the mononuclear ion pairs **11** and **12** were generated as brown oils (Scheme 3). Attempts to isolate or crystallize these complexes were unsuccessful and resulted in dark, solvent-retaining oils, a behavior not infrequently observed for metallocenium $[B(C_6F_5)_4]^-$ salts.[24] The ^{1}H NMR spectra of **11** and **12** at 10 °C show four distinct resonances for the C_5H_4 ring and two methyl signals for the CMe_2 bridge, in accord with C_1 symmetry (Figure 5). The chemical shift difference of the M−CH_2 signals (**11**, $\Delta\delta = 2.83$ ppm, $^2J_{HH} = 12$ Hz; **12**, $\Delta\delta = 2.53$ ppm, $^2J_{HH} = 12$ Hz; at 10 °C in 9:1 toluene-d_8−1,2-difluorobenzene) is reminiscent of that found for the SBI ligand system.[5,9] The ^{19}F spectrum of complex **11** shows no evidence for anion binding. For the hafnium complex **12** at 20 °C, the $SiMe_3$ signal is observed as a broad singlet which on cooling to −20 °C splits into two components at δ −0.15 and at −1.74 (2:1). This behavior mirrors that observed for $[(SBI)MCH_2SiMe_3^+\cdots B(C_6F_5)_4^-]$ (M = Zr (**13**), Hf (**14**)); that is, the rotation of the $SiMe_3$ moiety is slowed by an agostic interaction of one of the Si−Me groups with the metal center. This interaction is much

(21) For a definition of inner-sphere ion pairs (ISIPs) and outer-sphere ion pairs (OSIPs), see: Macchioni, A. *Chem. Rev.* **2005**, *105*, 2039.

(22) (a) Yang, X.; Stern, C. L.; Marks, T. J. *J. Am. Chem. Soc.* **1991**, *113*, 3623. (b) Deck, P. A.; Beswick, C. L.; Marks, T. J. *J. Am. Chem. Soc.* **1998**, *120*, 1772.

(23) (a) Bochmann, M.; Lancaster, S. J. *Angew. Chem., Int. Ed. Engl.* **1994**, *33*, 1634. (b) Bochmann, M.; Lancaster, S. J. *J. Organomet. Chem.* **1995**, *497*, 55.

(24) See for example: (a) Lee, H.; Hong, S. D.; Park, Y. W.; Jeong, B. G.; Nam, D. W.; Jung, H. Y.; Jung, M. W.; Song, K. H. *J. Organomet. Chem.* **2004**, *689*, 3402. (b) Stahl, N. G.; Salata, M. R.; Marks, T. J. *J. Am. Chem. Soc.* **2005**, *127*, 10898.

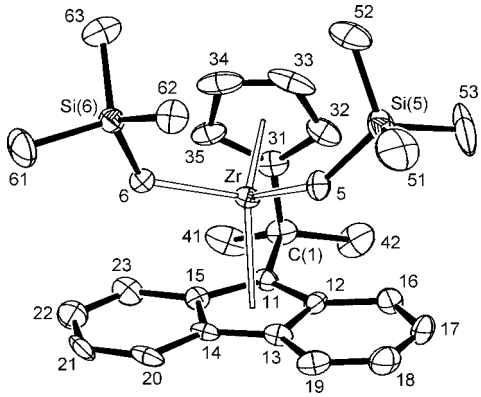

Figure 2. ORTEP representation of the structure of **1** showing 50% probability ellipsoids. Hydrogen atoms have been omitted for clarity. Selected bond lengths (Å) and angles (deg) with estimated standard deviations: Zr−Ct_{Flu} = 2.342, Zr−Ct_{Cp} = 2.187, Zr−C(5) = 2.237(6), Zr−C(6) = 2.259(6); Ct_{Cp}−Zr−Ct_{Flu} = 116.5, Ct(1)−Zr−C(5) = 108.8, Ct_{Flu}−Zr−C(6) = 108.5, Ct_{Cp}−Zr−C(5) = 112.5, Ct_{Cp}−Zr−C(6) = 109.0, C(5)−Zr−C(6) = 100.2(2), C(11)−C(1)−C(31) = 99.6(5), Zr−C(5)−Si(5) = 141.1(4), Zr−C(6)−Si(6) = 132.8(4). Ct_{Flu} and Ct_{Cp} are the centroids of the five-membered rings C(11−15) and C(31−35), respectively.

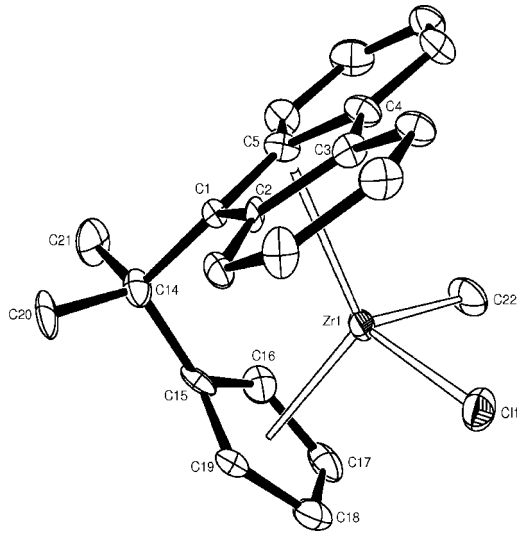

Figure 3. ORTEP representation of the structure of (IPCF)Zr(Me)Cl (**5**) showing 50% probability ellipsoids. Hydrogen atoms have been omitted for clarity; the dominant positions for C(22) and Cl(1) are shown. Selected bond lengths (Å) and angles (deg) with estimated standard deviations: Zr(1)−Cl(1) = 2.473(3), Zr(1)−C(22) = 2.19(2), Zr(1)−Ct_{Flu} = 2.268, Zr(1)−Ct_{Cp} = 2.174; C(22)−Zr(1)−Cl(1) = 98.3(10), mean plane [C(1)−C(5)]−mean plane [C(15)−C(19)] = 71.8(2).

stronger for Hf than Zr; in the case of **11** the decoalescence temperature could not be reached.

For the C_2-symmetric SBI ligand framework, chain swinging involves a 180° rotation of the alkyl ligand,[5] as indicated by the appearance of the M−CH^aH^b signals as a temperature-independent AB pattern; i.e., the methylene hydrogens do not interchange. In contrast, given the C_s-symmetric ligand framework in **11** and **12**, chain swinging involves a rotation by 120°. One would therefore expect H^a and H^b to interchange, and this is indeed observed; for example, the Hf−methylene signals of **12** coalesce at ca. 20 °C (Figures 5 and 6).

Site Epimerization Rates. The exchange processes in ion pairs **9**−**12** in the absence of olefin are conveniently followed by variable-temperature ^{1}H NMR spectroscopy, using the CMe_2 and Cp resonances as reporter signals. The ion pair symmetrization rate constants k_{ex} were calculated with the help of simulated spectra. ^{1}H NMR spectral data collected for **9**−**12** over a 40 K temperature range afforded kinetic parameters for both types of ion pairs. At a given temperature, k_{ex} was determined from the broadening of the bridge CMe_2 and the Cp resonances. Kinetic results are summarized in Table 1. The rates are dependent on (i) the metal, (ii) the Cp ligand, (iii) the counteranion, (iv) the solvent, (v) the alkyl ligand, and (vi) the ion pair concentration. Previously reported k_{ex} values for SBI systems[5] have been included for comparison.

It is well-known that exchange processes in $B(C_6F_5)_4^-$ compounds are faster than those in $MeB(C_6F_5)_3^-$ analogues.[1b,3b,8] The same trend was observed here for the ICPF ligand system; values of k_{ex} for the $B(C_6F_5)_4^-$ system are 2 orders of magnitude larger than for the inner-sphere $MeB(C_6F_5)_3^-$ compounds.

The site epimerization of (IPCF)ZrMe(μ-Me)$B(C_6F_5)_3$ in toluene has recently been investigated by Marks et al.[14b] In that case the main contribution to the overall rate was $B(C_6F_5)_3$ migration, whereas ion pair symmetrization was very slow: 0.8 s^{-1} at 77.5 °C. In contrast, for mixed-alkyl species such as **9** the borane migration pathway is not available, and the much higher k_{ex} value (3−16 s^{-1} at 20 °C, depending on [Zr]) is entirely due to ion pair reorganization. The greater fluxionality of **9** compared to that of (IPCF)Zr(μ-Me)$MeB(C_6F_5)_3$ clearly demonstrates the effect of steric hindrance provided by the bulky CH_2SiMe_3 ligand, which labilizes the anion.[25]

Another difference between the Zr−Me and the Zr−CH_2SiMe_3 systems is the concentration dependence of the site exchange process: whereas for (IPCF)ZrMe(μ-Me)$B(C_6F_5)_3$ k_{ex} was found to be independent of [Zr] over an 8-fold concentration range,[14b] the fluxionality of (IPCF)Zr(CH_2SiMe_3)(μ-Me)-$B(C_6F_5)_3$ (**9**) increases significantly with [Zr], from 3.2 ± 0.4 s^{-1} at [Zr] = 2 mM to 16 ± 2 s^{-1} at [Zr] = 20 mM. A similar concentration dependence was found for the Hf analogue **10**.

As observed previously,[14b] the ion pair [(IPCF)$ZrMe^+\cdots B(C_6F_5)_4^-$] was found to be too unstable to allow the determination of the rate of the dynamic reorganization process analogous to **11**. We note in passing that the site epimerization rate $k_{ex} \approx 11$ s^{-1} has been reported; however, this value was derived from a statistical analysis of the polypropylene microstructure and therefore relates to the mobility of the Zr−polymeryl species rather than to the Zr−Me ion pair.[26]

The zirconium and hafnium $MeB(C_6F_5)_3^-$ complexes **9** and **10** show closely comparable k_{ex} values. There is no significant difference between the SBI- and IPCF-derived complexes. On the other hand, when using $[Ph_3C][B(C_6F_5)_4]$ as a cocatalyst, the exchange rate of the SBI-containing system was higher than that of the IPCF-containing system by factors of ca. 1.5−2.5. The site epimerization rate for the hafnium $B(C_6F_5)_4^-$ ion pair **12** was significantly lower than for the Zr analogue **11**, most probably due to the stronger agostic interaction of Hf with the alkyl ligand.

The dependence of k_{ex} on the ion pair concentration of [(IPCF)$MCH_2SiMe_3^+\cdots B(C_6F_5)_4^-$] and [(SBI)$MCH_2SiMe_3^+\cdots$

(25) Acceleration of k_{ex} due to steric bulk of the alkyl ligand has been observed before in the series $(1,2\text{-}C_5H_4Me_2)_2ZrR(\mu\text{-Me})B(C_6F_5)_3$ (R = Me, CH_2Me_3, CH_2SiMe_3, $CH(SiMe_3)_2$). [22]

(26) A site epimerization rate of 11 s^{-1} at 60 °C given in ref 14b seems low compared to k_{ex} values found here for polymeryl models **11** and **12**. However, the reported value was based on a polymerization rate constant k_p that assumed no dormant states.[14b] Considering that kinetic procedures have shown that the active species concentration in most metallocene catalysts is typically 10−20% of total [Zr],[2a,13] the reported k_{ex} and k_p values are therefore likely to be underestimates by a factor of 5−10.

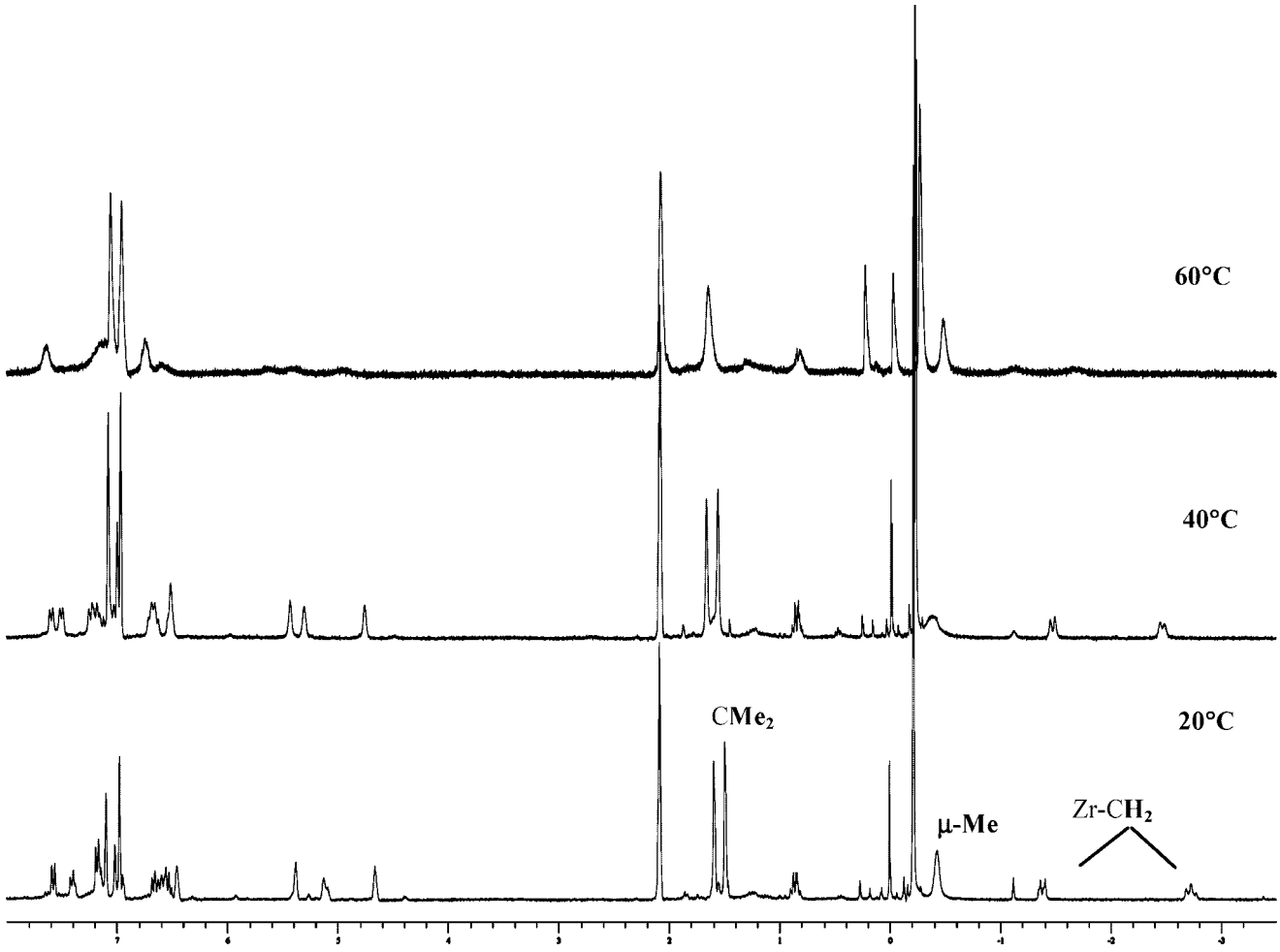

Figure 4. Variable-temperature ^{1}H NMR spectra of (IPCF)Zr(CH_2SiMe_3)(μ-Me)$B(C_6F_5)_3$ (**9**) in toluene-d_8 ([Zr] = 20 mM).

$B(C_6F_5)_4^-$] ion pairs is displayed in Table 2. The trends in k_{ex} are shown in Figure 7. The SBI ion pairs are less soluble than the IPCF analogues, which made it necessary to increase the amount of 1,2-difluorobenezene cosolvent from 10 to 20 vol %. Comparability between the IPCF and the SBI systems was established for the lowest [Zr], which could be determined in 9:1 toluene$-C_6H_4F_2$ for both types of compounds.

The starting point of this investigation was the significant difference we observed between the IPCF- and SBI-based propene polymerization catalysts, both in the catalyst productivities and, more particularly, in the response to increased trityl/Zr ratios. The site epimerization rates of **13** increase with increasing ion concentration over the observed range of [{A^+X^-}] = 2−50 mM. This increase is associated with the formation of ion aggregates.[5] The rate increase is understandable, since in an ion cluster the attraction of a given ion to a particular counterion is weakened by the presence of other ions in the immediate vicinity. Thus the ion quadruple $\{A^+X^-\}_2$ can dissociate into $A^+ \cdots \{X^-A^+X^-\}$, where $\{X^-A^+X^-\}$ represents a composite anion ("super anion") of reduced nucleophilicity (Scheme 4). This pathway is not open to a simple ion pair $\{A^+X^-\}$. Under the lower metal concentrations of catalytic batch reactions, the polymerization activity was also found to increase in line with the ion pair concentration (achieved by the addition of excess $[Ph_3C][B(C_6F_5)_4]$), up to a certain upper limit.[13]

Up to the site epimerization rate of $k_{ex} \approx 400\ s^{-1}$, the increase in rate for the IPCF ion pair **11** parallels the trend observed for the SBI analogue: i.e., both systems respond equally to the presence of other ion pairs in the system. However, whereas in the case of the SBI system the rate acceleration with increasing ion pair concentration continues almost linearly over the observed concentration range from 2 to 50 mM, up to $k_{ex} \approx 1400\ s^{-1}$ at 20 °C, there is no such rate increase for the IPCF system, and the exchange rate reaches a plateau.

This difference in fluxionality could be due to differences in ion aggregation, or it could indicate the detection of some barrier to site exchange that is operative in the IPCF system but absent in SBI compounds. In order to explore this in more detail, both the self-aggregation and the interionic structure of ion pairs **11** and **13** were investigated by pulsed-field gradient spin echo (PGSE) and NOE NMR experiments, respectively.

Interionic Structure of Ion Pairs by NOE and Diffusion NMR Experiments. The aggregation tendency of **11** and **13** in aromatic hydrocarbon solvents was recently investigated by means of ^{1}H and ^{19}F diffusion NMR measurements.[16] Diffusion coefficients (D_t), hydrodymanic volumes (V_H), and aggregation numbers (N)[27] are summarized in Table 3. The results indicate that both **11** and **13** display similar hydrodynamic dimensions, corresponding to the predominance of ion quadruples at a concentration of 7 mM (8:2 v:v toluene-$d_8-1,2$-$F_2C_6H_4$), in the absence of $[Ph_3C][B(C_6F_5)_4]$ (Table 3, entries 1 and 6). Addition of variable amounts of $[Ph_3C][B(C_6F_5)_4]$ to the zirconocene ion

(27) The aggregation number N is defined as V_H/V_H^{IP0}, where V_H is the actual hydrodynamic volume observed by PGSE NMR and V_H^{IP0} is the hydrodynamic volume of the single ion pair. For both **11** and **13**, V_H^{IP0} was estimated to be 965 Å^3.

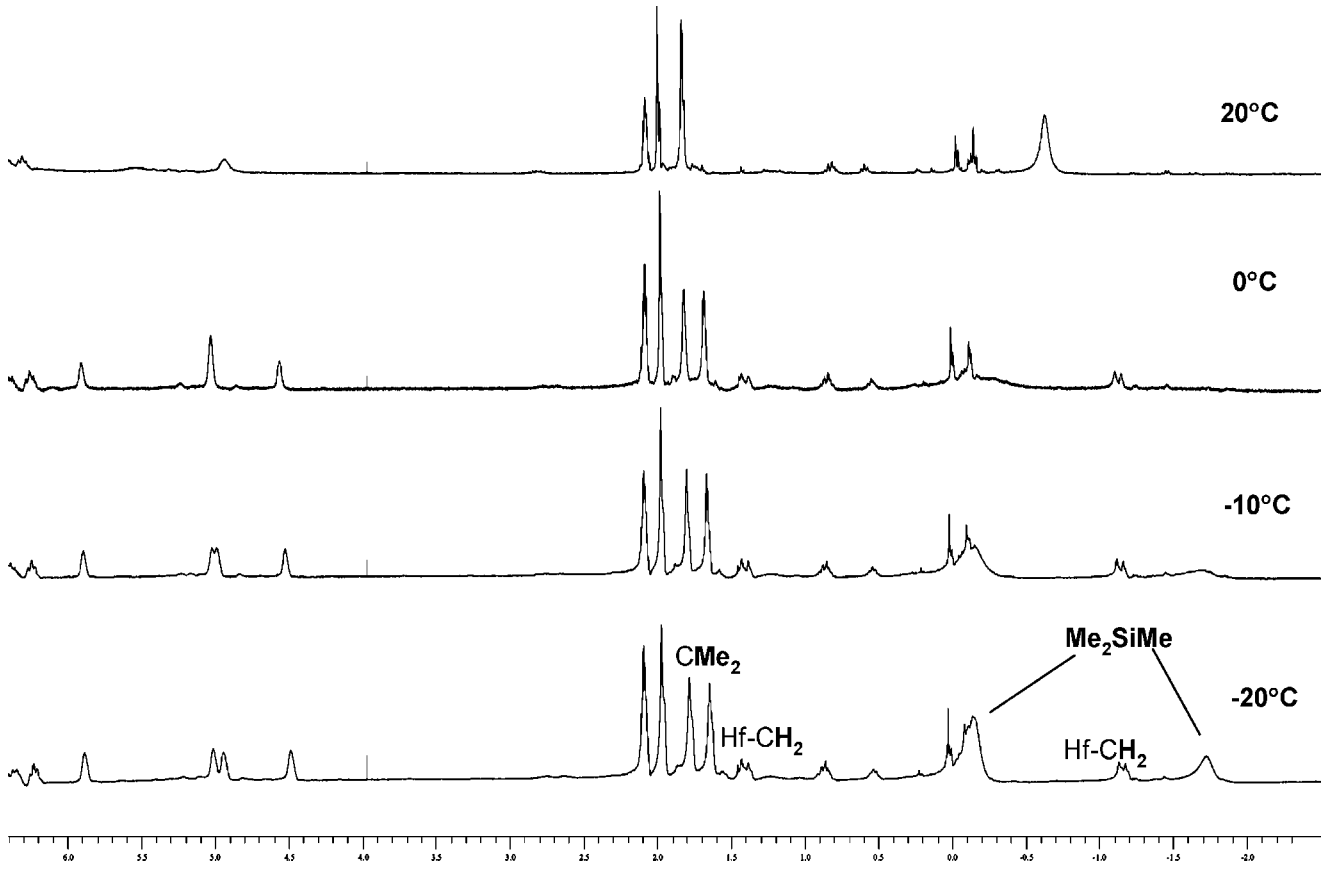

Figure 5. Variable-temperature ^{1}H NMR spectra of [(IPCF)Hf(CH_2SiMe_3)$^+ \cdots B(C_6F_5)_4^-$] (**12**) in 9:1 toluene-d_8−1,2-difluorobenzene ([Hf] = 20 mM).

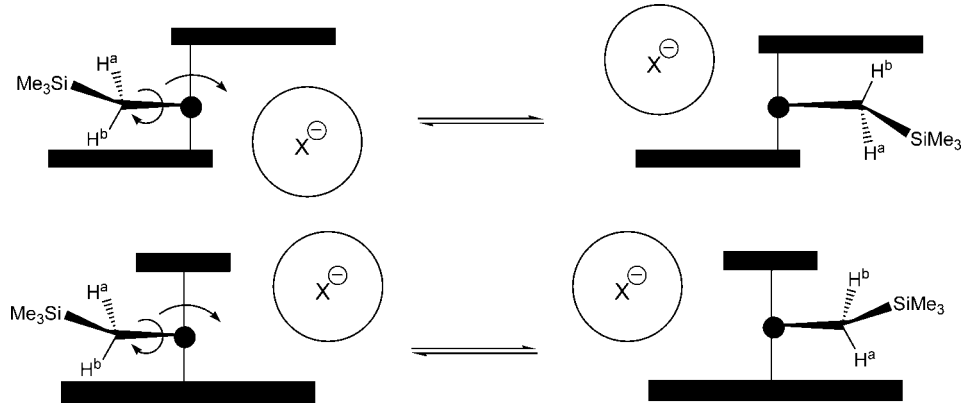

Figure 6. Stereochemistry of the chain swinging process involved in site epimerization: (a) for a C_2-symmetric ligand framework; (b) for C_s symmetry.

pairs results in a comparable increase of the hydrodynamic volume for both **11** and **13** (Table 3; compare entries 3 and 7). The last observation supports the notion of *mixed-ion aggregates* of the type [{$LZrR^+$}$_n${CPh_3^+}$_m${X^-}$_{n+m}$] being formed when an excess of [Ph_3C][$B(C_6F_5)_4$] is used. Importantly, both ion pairs **11** and **13** show a very similar tendency to form self-aggregates and mixed-ion aggregates. Consequently, the observed different dependence in site epimerization rates k_{ex}, and also in polymerization activities, on salt concentration is not related to detectably different aggregation tendencies of **11** and **13**.

Another factor that might influence the behavior of **11** and **13** could be the relative anion−cation positions, which in turn can determine the strength of the anion−cation interaction. Although PGSE experiments show that the two ion pairs have comparable values of the dipole moments and of the average cation−anion distances,[28] this does not imply that the relative cation−anion orientations within the ion pairs are the same.[29] To investigate the latter aspect, a series of ^{19}F,^{1}H HOESY experiments was carried out on **11** and **13**. Before ^{19}F,^{1}H HOESY experiments were performed, the levels of ion aggregation were evaluated by PGSE experiments in order to be sure that solutions of **11** and **13** were measured under identical aggregation conditions.

All the fluorine atoms of the anion show dipolar interactions with all the cationic aliphatic groups in the ^{19}F,^{1}H HOESY

(28) Zuccaccia, D.; Bellachioma, G.; Cardaci, G.; Ciancaleoni, G.; Zuccaccia, C.; Clot, E.; Macchioni, A. *Organometallics* **2007**, *26*, 3930.
(29) Macchioni, A. *Eur. J. Inorg. Chem.* **2003**, 195, and references therein.

Table 1. Site Epimerization Rate constants for Inner-Sphere and Outer-Sphere Zirconium and Hafnium Ion Pairs with IPCF and SBI Ligand Frameworks

cat.	[metal] (mM)	$C_6H_4F_2$ (vol %)	k_{ex} (s^{-1}) at 20 °C L = IPCF	k_{ex} (s^{-1}) at 20 °C L = SBI
(L)Zr(CH_2SiMe_3)(μ-Me)B(C_6F_5)$_3$	2	0	3.2 ± 0.4	14 ± 1
	20	0	16 ± 2	18 ± 1
(L)Hf(CH_2SiMe_3)(μ-Me)B(C_6F_5)$_3$	2	0	2.8 ± 0.4	21 ± 1.5
	20	0	21 ± 1	31 ± 2
	20	10	35 ± 2	
(L)Zr(μ-Me)MeB(C_6F_5)$_3$	2	0	0.4 ± 0.5	3 ± 0.6
(IPCF)Zr(μ-Me)MeB(C_6F_5)$_3$[a]	*b*	0	0.8 ± 0.4 (77.5 °C)[b]	
[(L)Zr(CH_2SiMe_3)$^+$ ··· B(C_6F_5)$_4^-$]	2	10	77 ± 100	351 ± 100
	20	10	435 ± 80	
	20	20		1048 ± 250
[(L)Hf(CH_2SiMe_3)$^+$ ··· B(C_6F_5)$_4^-$]	2	10	46 ± 100	180 ± 30
	20	10	250 ± 40	330 ± 60

[a] From ref 14b. [b] Independent of [Zr] over an 8-fold concentration range.

Table 2. Dependence of k_{ex} on the Ion Pair Concentration in the Systems (L)ZrMe(CH_2SiMe_3)/CPh_3[B(C_6F_5)$_4$] (L = IPCF, SBI) at Various CPh_3^+:Zr Ratios

[Zr] mM	[CPh_3^+]/[Zr]	total ion pair concn	toluene-d_8−$C_6H_4F_2$ (mL)	k_{ex} at 20 °C (s^{-1})
		L = SBI		
2	1	2	0.9:0.1	351 ± 100
10	1	10	0.8:0.2	613 ± 100
10	2	20	0.8:0.2	785 ± 100
10	3	30	0.8:0.2	1064 ± 250
10	4	40	0.8:0.2	1436 ± 400
20	1	20	0.8:0.2	1048 ± 250
		L = IPCF		
2	1	2	0.9:0.1	77 ± 100
5	1	5	0.9:0.1	160 ± 100
10	1	10	0.9:0.1	325 ± 70
10	2	20	0.9:0.1	448 ± 80
10	3	30	0.9:0.1	380 ± 80
10	4	40	0.9:0.1	448 ± 80
10	4	40	0.8:0.2	459 ± 80
20	1	20	0.9:0.1	435 ± 80

spectrum of **13** recorded at room temperature when ion quadruples are the main species present in solution (10 mM, 9:1 v:v toluene-d_8−1,2-$F_2C_6H_4$; $V_H = 2151$ Å^3, $N = 2.2$; Table 3, entry 8).[29] The interionic contacts involving the $SiMe_3$ moiety are the most intense, while those due to the bridging $SiMe_2$ and the Zr−CH_2 moieties are smaller and of similar intensity.[30] The interaction between the methylene proton resonating at higher frequency (H^a in Figure 6) and the anion, especially with the *o*-F nuclei, is stronger than that involving H^b. As shown in Figure 8A,B, the same interionic contacts, with similar relative intensities, are observed for solutions mainly containing ion pairs (52 mM, 1:2 v:v toluene-d_8−1,2-$F_2C_6H_4$; $V_H^+ = 1037$ Å^3; $N = 1.1$; Table 3, entry 9). These data suggest that the anion prefers to pair with the cation "laterally", from the same side where the methylene group lies, partly shifted toward the region of the space not occupied by the benzene rings of the indenyl ligands. In other words, it seems that structure **13-B** (see Figure 9) gives the main contribution to the overall average interionic structure. By comparison, in the ligand-stabilized outer-sphere ion pair [$Me_2SiCp_2ZrMe(THF)$][$MeB(C_6F_5)_3$] the anion was preferentially located away from the Me ligand.[4c]

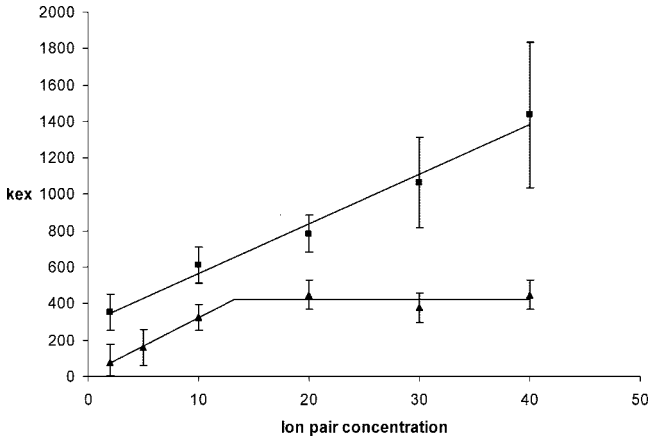

Figure 7. Site epimerization rate constants k_{ex} as a function of the ion pair concentration at 20 °C: (□) (SBI)ZrMe(CH_2SiMe_3)/[Ph_3C]$^+$[B(C_6F_5)$_4$]$^-$; (▲) (IPCF)ZrMe(CH_2SiMe_3)/[Ph_3C]$^+$[B(C_6F_5)$_4$]$^-$. Data are taken from Table 2.

Similar results are obtained for **11**. There are no appreciable differences between the room-temperature $^{19}F,^1H$ HOESY spectra of **11** recorded under conditions where ion pairs (40 mM, 4:6 v:v toluene-d_8−1,2-$F_2C_6H_4$; $V_H^+ = 913$ Å^3; $N = 0.9$; Table 3, entry 4) or ion quadruples (7 mM, 8:2 v:v toluene-d_8−1,2-$F_2C_6H_4$; $V_H^+ = 1766$ Å^3; $N = 1.8$; Table 3, entry 1) are the main species present in solution. Specifically, the interaction of the $SiMe_3$ group with the anion is stronger than that involving the CMe_2 bridge, while their relative ratio is similar to that observed in **13** for the $SiMe_3$ and $SiMe_2$ moieties. For **11**, the interionic contact with the Zr−CH_2 group cannot be detected at room temperature, since the resonances of the two methylene protons are extremely broad. A $^1H,^{19}F$ HOESY spectrum was then recorded at 270 K under conditions where ion pairs predominate in solution (20 mM, 1:1 v:v toluene-d_8−1,2-$F_2C_6H_4$; $V_H^+ = 1237$ Å^3; $N = 1.3$; Table 3, entry 5). Interionic contacts between the anion and the diasterotopic Zr−CH_2 protons become visible, but they are of lower intensity when compared with those observed for **13** (Figure 8C,D). Perhaps, in the case of **11**, the anion can approach the cation from both "lateral" sides, or in other words, the contributions of structures **11-A** and **11-B** (Figure 9) became comparable.

The ion pair **11-A** could be defined as an inner-sphere ion pair since a *m*-fluorine atom of the counterion stays very close to the metal (Figure 9). At the same time, the dipole moment of **11-A**, as well as its aggregation tendency, is not significantly different from that of the other ion pair geometries shown in Figure 9, since the Zr−B distances are almost the same. It can be speculated that the higher tendency of **11** to form the "inner-sphere"-type structure **11-A** makes the counterion in **11** on average more strongly bound than in **13**. Concerning its behavior in propene polymerizations, this may go some way to explain the lower dependence of the catalyst productivity of **11** on increasing its concentration and that of trityl borate, compared to the case for **13**.

Modeling of Ion Pair Geometries. The geometries and bonding of the IPCF and SBI ion pairs were explored using density functional theory (DFT) methods. For both systems **11** and **13** we located three geometries (Figure 9). Two of these show γ-agostic interactions between the alkyl ligand and the

(30) The experimental intensity of each interionic contact was corrected for the number of equivalent nuclei according to Macura and Ernst: Macura, S.; Ernst, R. R. *Mol. Phys.* **1980**, *41*, 95.

Scheme 4

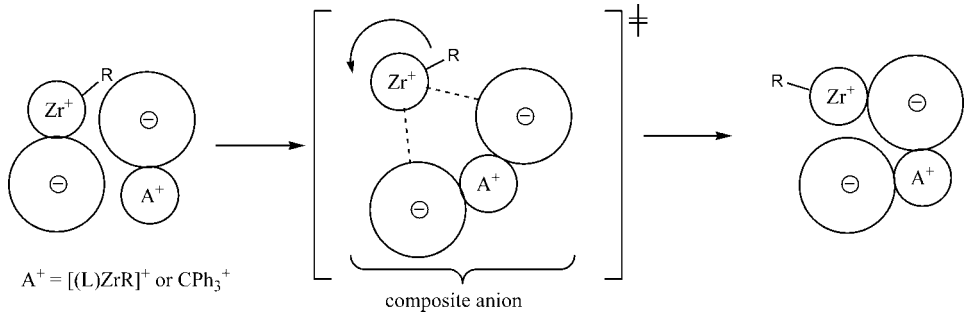

Table 3. Translational Diffusion Coefficient (D_t, 10^{-10} m^2 s^{-1}), Hydrodynamic Volumes (V_H, Å^3), and Aggregation Numbers (N) for [(IPCF)Zr(CH_2SiMe_3)][$B(C_6F_5)_4$] (11) and [(SBI)Zr(CH_2SiMe_3)][$B(C_6F_5)_4$] (13) Ion Pairs in the Presence or Absence of an Excess Amount of [Ph_3C][$B(C_6F_5)_4$]

entry	[Zr] (mM)	[Ph_3C][$B(C_6F_5)_4$] (mM)	toluene-d_8−1,2-$F_2C_6H_4$ (v:v)	D_t^+	D_t^-	V_H^+	V_H^-	N^+	N^-
			Ion Pair **11**						
1[a]	7		8:2	5.24	5.17	1766	1823	1.8	1.9
2[a]	7	14	8:2	4.87	4.83	1941	1979	2.0	
3[a]	7	28	8:2	4.43	4.51	2208	2115	2.3	
4	40		4:6	5.49		913		0.9	
5[b]	20		1:1	3.69		1237		1.3	
			Ion Pair **13**						
6[a]	7		8:2	5.32	5.31	1689	1697	1.8	1.8
7[a]	7	28	8:2	4.50	4.53	2135	2092	2.2	
8[c]	10		9;1	4.64		2151		2.2	
9	52		1:2	5.15		1037		1.1	

[a] From ref 16. [b] At 270 K. [c] From ref 5.

Zr atom,[32] with the outer-sphere anion either on the side of the Me groups ("front-side", structures **11-A** and **13-A**) or on the side of the CH_2 group ("back-side", structures **11-B** and **13-B**). In the third geometry, structures **11-C** and **13-C**, the γ-agostic interactions are replaced by a close approach of a *m*-F atom of the counteranion; the overall geometry corresponds more to an "inner-sphere" tight ion pair.

Within this general scheme, there are differences between the two ligand systems. While in geometries **B** and **C** the shortest F···Zr distances are quite similar (∼4.5 Å in **11-B** and **13-B** and ∼2.3 Å in **11-C** and **13-C**), in the front-side γ-agostic geometries **A** the minimum distance between the counterion and the Zr atom in **11-A** is ∼1.2 Å shorter than in **13-A** (∼3.1 Å vs ∼4.3 Å).

There are significant differences in the relative stabilities of the various geometries. For the SBI complex the front-side γ-agostic geometry **13-A** is the most stable, with a total interaction energy $E_{binding} = -17.9$ kcal mol^{-1} in benzene (see Table 4), whereas the back-side γ-agostic **13-B** geometry and the **13-C** geometry are slightly higher in energy, with $\Delta E_{binding} = 2.7$ and 1.3 kcal mol^{-1}, respectively. In contrast, for the IPCF ion pair **11** the inner-sphere geometry **C**, with a total interaction energy in benzene of −15.6 kcal mol^{-1}, was found to be slightly more stable (by 2.9 kcal mol^{-1}) than the γ-agostic geometries **11-A** and **11-B**. Comparison of the gas-phase interaction energies with those in benzene clearly indicates that even a low-polarity solvent such as benzene reduced the total interaction energies very significantly, from 35−40 kcal mol^{-1} to only ca. 15 kcal mol^{-1}. However, the *relative* interaction energies are scarcely dependent on solvent polarity; the greatest deviation is in the $\Delta E_{binding}$ value of **11-C**, which is 5.0 kcal mol^{-1} more stable than the **A** and **B** geometries in the gas phase. This dependence of the strength of the ion pair on solvent polarity was already pointed out by other authors.[31]

We also increased the solvent dielectric constant ϵ to 10: that is, approximately to the polarity of the solvent mixture used in the NMR experiments (ca. 1:2 toluene−*o*-difluorobenzene). These additional calculations resulted in a further clear decrease of the total interaction energies down to a few kcal mol^{-1} only, with a small flattening of the energy differences between the various geometries. Considering the limited basis set we used in the DFT calculations, we prefer to not include the specific numbers for $\epsilon = 10$ in Table 3, since they would be affected by a large percentage error. However, we can conclude that the DFT calculations suggest (a) that the three geometries are of quite similar energy and (b) that in high-polarity solvent the interaction energies are rather small and, thus, both ion pairs can probably fluctuate between the various geometries. The small energy differences we found suggest that the effects of ion aggregation (which for reasons of computational complexity are not modeled here) may well be able to shift the balance in favor of geometries **A** or **B**, as was found in the experimental studies.

Geometric analysis and decomposition of the interaction energies (see the Supporting Information for details) suggest that the origin of this different behavior is related to a higher flexibility of the metallocene skeleton of **11**. In fact, on going from the naked cation to the ion pair there is a tendency of the Flu ligand to slip from a mainly η^5 coordination toward an η^3 coordination. This finding is in qualitative agreement with the propensity of fluorenyl ligands to decrease the hapticity.[33] The change in hapticity increases the bite angle of the metallocene to accommodate the counterion in **11** more effectively than in **13**.

(31) (a) Xu, Z.; Vanka, K.; Firman, T.; Michalak, A.; Zurek, E.; Zhu, C.; Ziegler, T. *Organometallics* **2002**, *21*, 2444. (b) Xu, Z.; Vanka, K.; Ziegler, T. *Organometallics* **2004**, *23*, 104. (c) Lanza, G.; Fragalà, I. L.; Marks, T. J. *J. Am. Chem. Soc.* **2000**, *122*, 12764. (d) Lanza, G.; Fragalà, I. L.; Marks, T. J. *Organometallics* **2002**, *21*, 5594. (e) Tomasi, S.; Razavi, A.; Ziegler, T. *Organometallics* **2007**, *26*, 2024.

(32) For calculations on the structures of related Bu^i-Zr complexes and the relative energies of β-and γ-agostically bonded alkyl ligands see ref 31e.

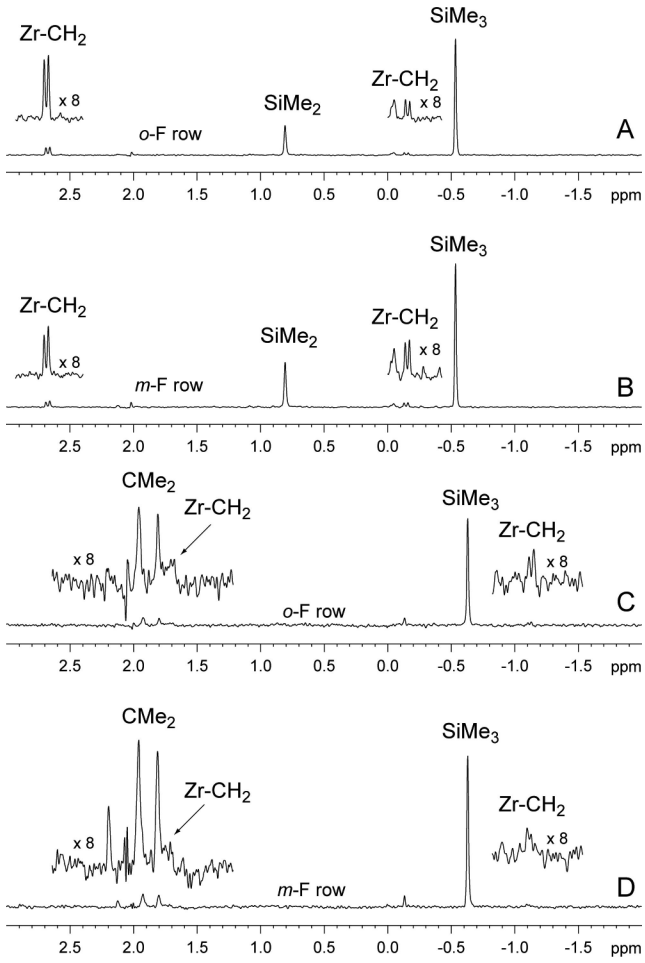

Figure 8. (A, B) Two slices of the $^{1}H,^{19}F$ HOESY NMR spectrum of **13** relative to the *o*- and *m*-fluorine resonances, respectively (298 K, 52 mM, 1:2 v:v toluene-d_8−1,2-$F_2C_6H_4$, mixing time 500 ms). (C, D) Two slices of the $^{1}H,^{19}F$ HOESY NMR spectrum of **11** relative to the *o*- and *m*-fluorine resonances, respectively (270 K, 20 mM, 1:1 v:v toluene-d_8−1,2-$F_2C_6H_4$, mixing time 500 ms).

The dynamics of ion pair formation from the solvent-separated ions was probed using molecular dynamics (MD) simulations of the two systems, which were performed using a classical molecular mechanics (MM) force field that had to be parametrized to the scope. The developed force field was then used to perform MD simulations of both ion pairs. Details about force field parametrization are reported in the Supporting Information. We focused particularly on the analysis of the **A** and **C** geometries of both **11** and **13**. The main aim was to compare the dynamic behavior of ion pairs in the **A** and **C** geometries, which are the geometries that present the counterion on the side of the agostic interaction.

Each ion pair was swollen in a box containing roughly 1600 benzene molecules and was equilibrated at 300 K and 1 atm. After equilibration, production runs of the two systems were performed for a total time of 1000 ps. For both the **11** and **13** systems, the simulations performed starting from the different minima **A** and **C** converged to a unique structure with a unique dynamics behavior after a few picoseconds. For this reason, we will limit the discussion only to trajectories started from the **C** geometry of both ion pairs.

The plots of Figure 10 report the shortest Zr···F and Zr−γ-Me distances for both ion pairs. We first discuss the MD simulation of **13** (right side of Figure 10). The plot clearly indicates that the geometry of system **13**, with a Zr···F distance ~4 Å and a γ-agostic interaction of ca. 3.5 Å, is rather stable over time. Indeed, both distances fluctuate around the average value, and the shortest Zr···F distance always involves a *m*-F atom.

In contrast, the dynamic behavior of the ion pair **11** is rather more complex. Already during equilibration we found that one of the γ-Me groups strongly approaches the metal, almost establishing a γ-agostic interaction. Moving to the sampled configurations (left-hand plot in Figure 10), it is clear that at short simulation times (around 100 ps) one *m*-F atom, labeled F1, strongly approaches the metal, while the peak of the Zr···γ-Me distance at almost 5 Å indicates that the γ-agostic interaction is almost broken. Further, around 300−400 ps there is a conformational rearrangement, and the *m*-F1 atom is substituted by the *m*-F2 (atom which belongs to a different C_6F_5 ring) in the first coordination sphere of the metal. This rearrangement does not involve the γ-agostic interaction. In short, our MD analysis indicates that the (weakly α-agostic) geometry **11-C** is unstable dynamically and that a geometry more consistent with the γ-agostic structure **11-A** is adopted. This is despite the fact that geometry **11-C** is favored by more than 5 kcal mol^{-1} by static calculations in the gas phase.

Further insight can be obtained by reporting in the same plot the shortest Zr···F distance in both the **11** and **13** ion pairs. In this case, we are not interested in which specific F atom coordinates to the metal,; rather, we focus on the geometry of the metal coordination sphere. The plot reported on the left in Figure 11 indicates that, with the exception of a short picosecond window (100−200 ps), the shortest Zr···F distance is always 0.5−1.0 Å shorter in **11**, which is in agreement with the QM calculations that **11** presents a somewhat more tightly bound counterion. Of course, in the case of **11** the plot of Figure 10a indicates that there is a change in which specific F atom is closest to the metal during the simulation. On the other hand, a similar analysis performed on the Zr···γ-Me distances, reported on the right side of Figure 11, indicates that very similar Zr···γ-Me distances are observed in the MD simulations of both ion pairs. In conclusion, the MD simulations suggest that the dynamics of both systems are consistent with a geometry in which a methyl group of the $-CH_2SiMe_3$ ligand is involved in a γ-agostic interaction, and one *m*-F atom is within 3.5 Å (**11**) or 4.5 Å (**13**). There is a slightly tighter anion binding in the case of IPCF complexes.

Conclusions

The mixed-alkyl complexes (IPCF)M(Me)(CH_2SiMe_3) (M = Zr, Hf) are accessible from the dichlorides by a three-step procedure, which is necessitated by the poor solubility of (IPCF)MCl_2. Subsequent treatment of the dialkyls with $B(C_6F_5)_3$ or $[Ph_3C][B(C_6F_5)_4]$ leads to selective methyl abstraction and formation of inner-sphere and outer-sphere ion pairs, respectively. The inner-sphere ion pairs (IPCF)M(CH_2SiMe_3)(μ-Me)$B(C_6F_5)_3$ undergo site epimerization without competing borane exchange. These rates not only are significantly faster than those of the analogous metal−methyl complexes but also differ from these methyl species in being strongly concentration dependent.

The tetraarylborates [(IPCF)M−$CH_2SiMe_3^+$···$B(C_6F_5)_4^-$] are significantly more thermally stable than the M−CH_3 analogues. As is the case for the SBI ion pairs, alkyl ligand

(33) (a) Bochmann, M.; Lancaster, S. J.; Hursthouse, M. B.; Mazid, M. *Organometallics* **1993**, *12*, 4718. (b) Irvin, L. J.; Miller, S. A. *J. Am. Chem. Soc.* **2005**, *127*, 9972.

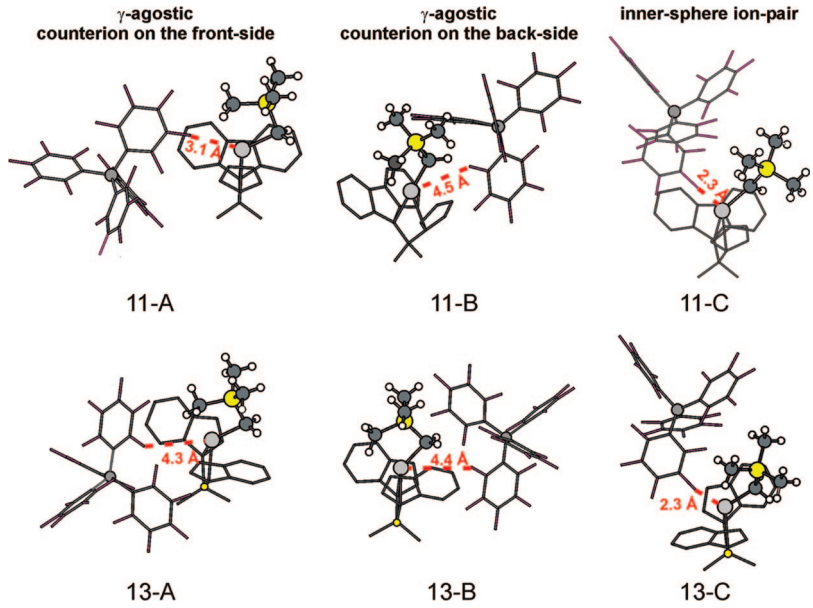

Figure 9. DFT minimum energy geometries of ion pairs **11** and **13**.

Table 4. Total Interaction Energies, $E_{binding}$, and Relative Interaction Energies, $\Delta E_{binding}$, with Respect to the A Geometry for Systems 11 and 13[a]

	gas phase (ϵ = 1.0)		benzene (ϵ = 2.8)	
geom	$E_{binding}$	$\Delta E_{binding}$	$E_{binding}$	$\Delta E_{binding}$
11-A	−35.7	0.0	−12.7	0.0
11-B	−35.7	0.0	−12.5	0.2
11-C	−40.6	−5.0	−15.6	−2.9
13-A	−41.1	0.0	−17.9	0.0
13-B	−38.4	2.7	−15.1	2.7
13-C	−39.2	1.2	−16.6	1.3

[a] All values are givein in kcal mol^{-1}.

binding is characterized by an agostic interaction with a Si−Me moiety. The preference for this bonding type, in favor of tight anion binding, is borne out by DFT calculations; these also suggest that the more flexible IPCF ligand may permit slightly tighter binding of the $B(C_6F_5)_4^-$ anion than does the SBI ligand. These structures are also the minimum energy geometries derived from molecular dynamics simulations over a 1000 ps time frame.

Increasing the ion concentration leads to increased site epimerization rates k_{ex}; this can be achieved either by increasing [Zr] at a constant CPh_3^+:Zr ratio of 1:1 or by increasing the $[Ph_3C][B(C_6F_5)_4]$ content. PGSE NMR measurements show that the increase in k_{ex} is paralleled by an increase in the concentration of ion quadruples. Thus, these data support the notion of mixed-ion aggregates $[\{LZrR^+\}_n\{CPh_3^+\}_m\{X^-\}_{n+m}]$ being formed when the trityl:Zr ratio exceeds 1:1. In such aggregates, ion separation may be made more facile by dissociation into species such as $[(L)ZrR^+]\cdots[X^-CPh_3^+X^-]$, which is reflected in the increased site epimerization rates. Under catalytic conditions, such a response to the presence of additional $[Ph_3C][B(C_6F_5)_4]$ would result in an activity increase.

Up to $k_{ex} \approx 400$ s^{-1} (at 20 °C) the response of the IPCF system to increased ion pair concentration mirrors that of the analogous SBI compounds. However, whereas in the SBI system k_{ex} continues to increase linearly with total ion pair concentration, the site epimerization rates for IPCF complexes reach a plateau. Together with the PGSE NMR results, the data suggest that none of the possible explanations put forward in the Introduction for the lack of "trityl effect" in the IPCF catalyst system applies, and we believe the most probable explanation for the limit imposed on dynamic processes in this case are ligand-dependent steric factors. We feel this behavior goes some way in explaining the strong positive "trityl effect" in SBI and related catalysts and the lack of such a response in others, including the IPCF system. These results demonstrate that the determination of site epimerization rates as a function of ion pair concentration can be used to detect unexpected rate-limiting barriers to ligand fluxionality in metallocene catalysts.

The question remains to what extent the influences on site epimerization rates discussed above have a bearing on the processes involved in polymer chain growth. Some steps such as the chain-swinging event are common to both processes, as indicated in Scheme 1, and it is reasonable to suggest that steric barriers that affect the rate with which an alkyl ligand can move from one side of the catalyst to the other in site epimerization will also be relevant during alkyl migration to a coordinated monomer. Since polymerizations are faster than site epimerization, it is to be expected that under catalytic conditions this upper limit on ligand fluxionality is reached at much lower [Zr]; this would explain the observed lack of response of IPCF catalysts to increased doses of trityl activator, while metallocenes where such a barrier can be shown to be absent experience a significant activity enhancement.

The understanding of the solution structures and dynamics of metallocenium ion pairs is greatly assisted by static and dynamic calculations. The comparison among experimental results, static calculations, and molecular dynamics simulations clearly indicates that static methods (like classical geometry optimizations) are probably not the most effective tool to study ion pair structural properties, at least in cases where several geometries have to be considered which are structurally quite different but have rather similar energies. In these problematic situations additional dynamics simulations can provide a more complete chemical scenario.

Experimental Section

General Procedures. All manipulations were performed under dry nitrogen gas using standard Schlenk techniques. Solvents were purified by distillation under nitrogen from sodium−potassium alloy (light petroleum, bp 40−60 °C), sodium (low-sulfur toluene) or

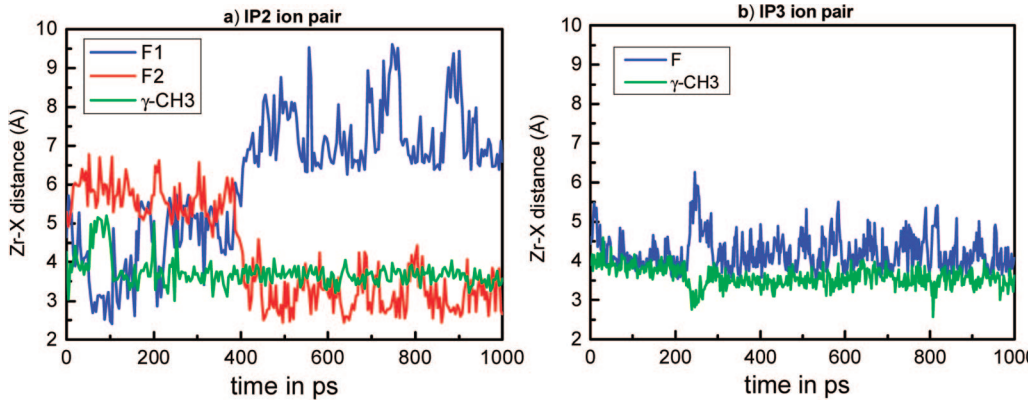

Figure 10. Plots of the shortest Zr···F and Zr···γ-Me distances in ion pairs **11** (a) and **13** (b).

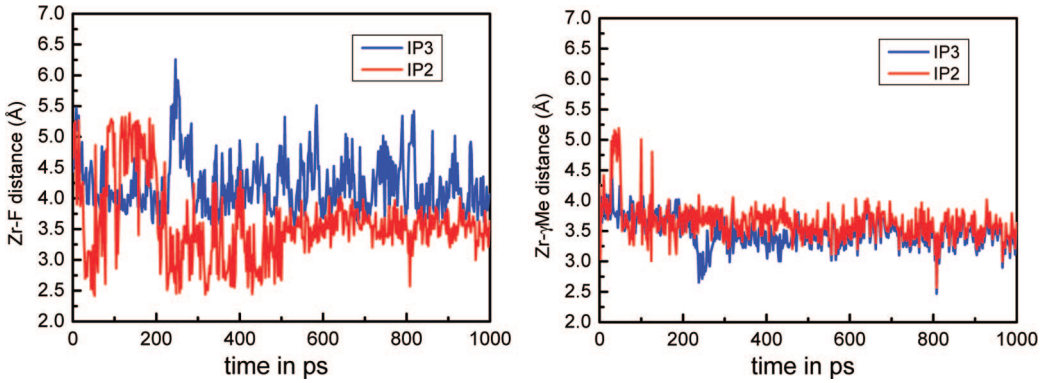

Figure 11. Shortest Zr···F (left) and Zr···γ-Me (right) distances in the ion pairs **11** (red) and **13** (blue).

sodium-benzophenone (THF). $[Ph_3C][B(C_6F_5)_4]$ was synthesized from Ph_3CCl with $Li[B(C_6F_5)_4]$ in dichloromethane and recrystallized from a dichloromethane−light petroleum solvent mixture to afford a yellow crystalline solid in 97% yield.[34] $Li[B(C_6F_5)_4]$ was made from $B(C_6F_5)_3$ and LiC_6F_5 in light petroleum[35] and was free from other borate impurities within NMR detection limits (^{19}F, ^{11}B) without further purification. The compounds (IPCF)MMe_2 (M = Zr (**3**), Hf (**4**)) were synthesized following literature procedures.[17] The ion pair $[(SBI)ZrCH_2SiMe_3^+ \cdots B(C_6F_5)_4^-]$ (**13**) was prepared as described.[5,9] Deuterated toluene was dried by stirring over Na/K alloy followed by trap-to-trap distillation; 1,2-$F_2C_6H_4$ was degassed and dried over activated 4 Å molecular sieves. NMR (^1H, ^{13}C, ^{19}F, ^{11}B) spectra were recorded on a Bruker Avance DPX-300 spectrometer; PGSE NMR measurements were performed on a Bruker Avance DRX-400 instrument. Chemical shifts were referenced to residual solvent peaks (^1H, ^{13}C), $CFCl_3$ (^{19}F), or $BF_3 \cdot OEt_2$ (^{11}B).

Variable-temperature NMR spectra of ion pairs were recorded at temperature intervals of 5 °C over a range from 20 to 60 °C (compounds **9** and **10**) and −20 to 20 °C (compounds **11** and **12**). The acquisition relaxation delay (d1) was 12 s and time domain size 65 536 data points. A total of 32−64 scans were accumulated (^1H). Spectra were simulated using the gNMR program (version 4.1). Rate constants at each temperature were estimated by visual matching of line shapes of simulated and experimental spectra.

Preparation of (IPCF)Zr(CH_2SiMe_3)$_2$ (1). A suspension of (IPCF)$ZrCl_2$ (1.5 g, 3.5 mmol) in toluene (100 mL) was treated with $ClMgCH_2SiMe_3$ (6 mL of a 1.2 M solution in diethyl ether, 7.2 mmol). The mixture was stirred overnight at room temperature. After removal of the volatiles in vacuo, the residue was extracted with light petroleum (30 mL). Concentration of the resulting solution and cooling to −25 °C overnight yielded yellow needles suitable for X-ray crystallography (1.0 g, 1.9 mmol, 53%). Anal. Calcd for $C_{29}H_{40}Si_2Zr$: C, 64.98; H, 7.52. Found: C, 64.46; H, 7.09. ^1H NMR (300 MHz, 25 °C, benzene-d_6): δ 7.81 (d, J = 8.3 Hz, 2H, Flu), 7.37 (d, J = 8.9 Hz, 2H, Flu), 7.22 (t, J = 8.2 Hz, 2H, Flu), 6.90 (t, J = 8.2 Hz, 2H, Flu), 6.40 (t, J = 2.5 Hz, 2H, C_5H_4), 5.42 (t, J = 2.5 Hz, 2H, C_5H_4), 1.73 (s, 6H, CMe_2), 0.03 (s, 18H, $SiMe_3$), −1.37 (d, J = 11.5 Hz, 2H, $ZrCH_2$), −2.16 (d, J = 11.5 Hz, 2H, $ZrCH_2$). ^{13}C NMR (75.47 MHz, 25 °C, benzene-d_6): δ 127.1, 123.8, 123.7, 122.3, 121.4, 111.5 (Flu), 110.7, 101.5, 77.6 (C_5H_4), 47.2 (J_{CH} = 103 Hz, $ZrCH_2$), 39.7 (CMe_2), 28.7 (CMe_2), 2.9 ($SiMe_3$).

Preparation of (IPCF)Hf(CH_2SiMe_3)$_2$ (2). A solution of (IPCF)H_2 (9.0 g, 33 mmol) was dissolved in cold (−78 °C) tetrahydrofuran (200 mL) and treated with *n*-butyllithium (41 mL of 1.6 M solution in hexanes, 66 mmol). The solution was warmed to room temperature and stirred for 1 h. Removal of the volatiles gave a dark red solid. The dianion was suspended in toluene (200 mL), $HfCl_4$ (33 mmol) was added, and the mixture was stirred overnight. The resulting suspension was treated with $ClMgCH_2SiMe_3$ (141 mL of a 0.72 M solution in diethyl ether, 100 mmol). Sufficient diethyl ether was removed under reduced pressure to allow the mixture to be heated to 80 °C for 16 h without reflux. Removal of the volatiles gave a sticky orange solid. Extraction with light petroleum (200 mL), concentration to 40 mL, and cooling to −25 °C gave yellow crystals, which proved to be contaminated with magnesium alkyl. This crude material was dissolved in toluene (40 mL) and treated with excess $ClSiMe_3$ at 70 °C over a period of 16 h. The toluene was then removed under vacuum and the product extracted with light petroleum (60 mL). Concentration and cooling to −25 °C yielded yellow-orange needle-shaped crystals of **2** (two crops, 5.0 g, 8.0 mmol, 24%). Anal. Calcd for $C_{29}H_{40}Si_2Hf$: C, 55.88; H, 6.47. Found: C, 55.52; H, 6.36. ^1H NMR (300 MHz, 25 °C, benzene-d_6): δ 7.80 (d, J = 8.3 Hz, 2H, Flu), 7.42 (d, J = 8.9 Hz,

(34) Bochmann, M.; Lancaster, S. J. *J. Organomet. Chem.* **1992**, *434*, C1.

(35) (a) Massey, A. G.; Park, A. J.; Stone, F. G. A. *Proc. Chem. Soc. London* **1963**, 212. (b) Massey, A. G.; Park, A. J. *J. Organomet. Chem.* **1964**, *2*, 245.

2H, Flu), 7.23 (t, $J = 8.2$ Hz, 2H, Flu), 6.89 (t, $J = 7.5$ Hz, 2H, Flu), 6.32 (t, $J = 2.5$ Hz, 2H, C_5H_4), 5.39 (t, $J = 2.5$ Hz, 2H, C_5H_4), 1.76 (s, 6H, CMe_2), 0.03 (s, 18H, $SiMe_3$), −1.84 (d, $J = 11.9$ Hz, 2H, $HfCH_2$), −2.52 (d, $J = 11.9$ Hz, 2H, $HfCH_2$). ^{13}C NMR (75.47 MHz, 25 °C, benzene-d_6): δ 127.3, 123.9, 123.5, 123.2, 122.2, 122.6, 114.5 (Flu), 110.57, 100.5, 79.0 (C_5H_4), 48.4 (d, $J_{CH} = 103$ Hz, $HfCH_2$), 39.7 (CMe_2), 28.8 (CMe_2), 3.6 ($SiMe_3$).

Preparation of (IPCF)Zr(Me)Cl (5). A solution of Ph_3CCl (0.68 g, 2.43 mmol) in toluene at 50 °C was added dropwise to a solution of **3** (1.0 g, 2.55 mmol) and maintained at this temperature over a period of 2 h. The resulting orange solution was cooled to 25 °C, and the volatiles were removed under vacuum. The resulting orange solid residue was washed with light petroleum (2 × 50 mL) and recrystallized from toluene at −25 °C to give the title compound as orange crystals suitable for X-ray analysis (0.96 g, 2.32 mmol, 95%). ^1H NMR (300 MHz, 25 °C, CD_2Cl_2): δ 8.18 (d, $J = 3.7$ Hz, 1H, Flu), 8.15 (d, $J = 3.7$ Hz, 1H, Flu), 7.84 (d, $J = 8.2$ Hz, 1H, Flu), 7.76 (d, $J = 8.2$ Hz, 1H, Flu), 7.50 (t, $J = 6.7$ Hz 1H, Flu), 7.43 (t, $J = 6.7$ Hz, 1H, Flu), 7.24 (t, $J = 7.2$ Hz, 1H, Flu), 7.22 (t, $J = 7.2$ Hz, 1H, Flu), 6.42 (m, 1H, C_5H_4), 6.02 (m, 1H, C_5H_4), 5.83 (m, 1H, C_5H_4), 5.54 (m, 1H, C_5H_4), 2.26 (s, 3H, CMe_2), 2.21 (s, 3H, CMe_2), −1.19 (s, 3H, ZrMe). ^{13}C NMR (75.47 MHz, 25 °C, CD_2Cl_2): δ 128.8, 127.8, 125.3, 124.8, 124.7, 123.8, 123.3, 122.6, 113.2 (Flu), 116.7, 115.3, 102.7, 101.1, 79.7 (C_5H_4), 40.8 (CMe_2), 34.9 (ZrMe), 28.9, 29.0 (CMe_2).

Preparation of (IPCF)Hf(Me)Cl (6). A solution of Ph_3CCl (0.55 g, 1.95 mmol) in toluene was added dropwise to a solution of **4** (1.0 g, 2.09 mmol) at 70 °C and maintained at this temperature over a period of 16 h. Workup following the procedure described for **5** gave the title compound **6** as orange crystals (0.69 g, 1.39 mmol, 70%). ^1H NMR (300 MHz, 25 °C, CD_2Cl_2): δ 8.11 (d, $J = 3.9$ Hz, 1H, Flu), 8.14 (d, $J = 3.9$ Hz, 1H, Flu), 7.90 (d, $J = 8.9$ Hz, 1H, Flu), 7.80 (d, $J = 8.9$ Hz, 1H, Flu), 7.49 (t, $J = 6.6$ Hz, 1H, Flu), 7.41 (t, $J = 6.6$ Hz 1H, Flu), 7.22 (t, $J = 7.0$ Hz, 1H, Flu), 7.18 (t, $J = 7.0$ Hz, 1H, Flu), 6.35 (m, 1H, C_5H_4), 5.93 (m, 1H, C_5H_4), 5.87 (m, 1H, C_5H_4), 5.47 (m, 1H, C_5H_4), 2.33 (s, 3H, CMe_2), 2.26 (s, 3H, CMe_2), −1.40 (s, 3H, HfMe). ^{13}C NMR (75.47 MHz, 25 °C, CD_2Cl_2): δ 128.7, 128.2, 124.9, 124.9, 124.2, 123.7, 122.6, 122.1, 115.7 (Flu). 116.3, 114.8, 101.0, 99.8, 80.4 (C_5H_4), 41.0 (CMe_2), 35.6 (HfMe), 29.6, 29.3 (CMe_2).

Preparation of (IPCF)Zr(Me)CH_2SiMe_3 (7). To a solution of **5** (0.96 g, 2.32 mmol) in toluene was added dropwise $ClMgCH_2SiMe_3$ (2.0 mL of a 1.4 M solution in diethyl ether, 2.80 mmol) at room temperature. The mixture was stirred over a period of 2 h. The solvents were removed under vacuum, and the product was extracted with light petroleum (60 mL). Removal of volatiles gave **7** as a yellow crystalline solid (0.81 g, 1.76 mmol, 76%). Anal. Calcd for $C_{26}H_{32}SiZr$: C, 67.32; H, 6.95. Found: C, 67.18; H, 6.82. ^1H NMR (300 MHz, 25 °C, benzene-d_6): δ 7.94 (d, $J = 8.9$ Hz, 1H, Flu), 7.87 (d, $J = 8.9$ Hz, 1H, Flu), 7.33 (d, $J = 8.3$ Hz, 1H, Flu), 7.29 (d, $J = 8.3$ Hz, 1H, Flu), 7.20 (t, $J = 6.7$ Hz, 2H, Flu), 6.89 (t, $J = 7.6$ Hz, 1H, Flu), 6.24 (t, $J = 7.6$ Hz, 1H, Flu), 6.24 (m, 1H, C_5H_4), 6.05 (m, 1H, C_5H_4), 5.18 (m, 1H, C_5H_4), 5.15 (m, 1H, C_5H_4), 1.70 (s, 3H, CMe_2), 1.67 (s, 3H, CMe_2), 0.00 (s, 9H, $SiMe_3$), −0.67 (d, $^2J = 11.9$ Hz, 1H, $ZrCH_2$), −1.23 (s, 3H, ZrMe), −2.31 (d, $^2J = 11.9$ Hz, 1H, $ZrCH_2$). ^{13}C NMR (75.47 MHz, 25 °C, benzene-d_6): δ 127.2, 127.0, 124.4, 124.3, 124.0, 124.0, 123.9, 122.9, 122.3, 121.8, 120.5, 120.0, 110.7 (Flu), 114.1, 112.0, 101.5, 100.9, 77.4 (C_5H_4), 46.2 ($ZrCH_2$), 40.0 (CMe_2), 35.9 (ZrMe), 28.8, 28.6 (CMe_2), 3.0 ($SiMe_3$).

Preparation of (IPCF)Hf(Me)CH_2SiMe_3 (8). To a solution of **6** (0.69 g, 1.38 mmol) in toluene was added $ClMgCH_2SiMe_3$ (1.2 mL of a 1.4 M solution in diethyl ether, 1.66 mmol) at room temperature. The mixture was stirred over a period of 16 h at 70 °C. The solvents were removed under vacuum, and the product was extracted with light petroleum (60 mL). The toluene was then removed under vacuum and the product extracted with light petroleum (60 mL). Concentration and cooling to −25 °C yielded **8** as a yellow crystalline solid (0.52 g, 0.95 mmol, 69%). Anal. Calcd for $C_{26}H_{32}SiHf$: C, 56.66; H, 5.85. Found: C, 56.56; H, 5.73. ^1H NMR (300 MHz, 25 °C, benzene-d_6): δ 7.94 (t, $J = 8.9$ Hz, 2H, Flu), 7.45 (d, $J = 8.9$ Hz, 1H, Flu), 7.40 (d, $J = 8.9$ Hz, 1H, Flu), 7.27 (t, $J = 7.8$ Hz, 2H, Flu), 6.94 (t, $J = 7.5$ Hz, 1H, Flu), 6.87 (t, $J = 7.5$ Hz, 1H, Flu), 6.20 (m, 1H, C_5H_4), 6.04 (m, 1H, C_5H_4), 5.21 (m, 1H, C_5H_4), 5.18 (m, 1H, C_5H_4), 1.73 (s, 3H, CMe_2), 1.71 (s, 3H, CMe_2), 0.06 (s, 18H, $SiMe_3$), −1.20 (d, $^2J = 12.3$ Hz, 1H, $HfCH_2$), −1.39 (s, 3H, HfMe), −2.43 (d, $^2J = 12.3$ Hz, 1H, $HfCH_2$). ^{13}C NMR (75.47 MHz, 25 °C, benzene-d_6): δ 126.3, 126.2, 123.4, 123.2, 122.8, 122.6, 122.5, 121.8, 121.2, 120.7, 118.5, 118.1 110.6 (Flu), 112.8, 112.7, 99.4, 98.7, 77.8 (C_5H_4), 48.4 ($HfCH_2$), 40.3 (CMe_2), 39.1 (HfMe), 28.0, 27.7 (CMe_2), 2.0 ($SiMe_3$).

Preparation of (IPCF)Zr(CH_2SiMe_3)(μ-Me)B(C_6F_5)$_3$ (9). A sample of **7** (9 mg, 0.020 mmol) and solid $B(C_6F_5)_3$ (10 mg, 0.020 mmol) were loaded into a 5 mm NMR tube and dissolved in 1 mL of toluene-d_8. The conversion to **9** was quantitative. There was no change in the NMR spectra of solutions kept in sealed tubes at room temperature for a period of several days. ^1H NMR (300 MHz, 25 °C, toluene-d_8): δ 7.62 (d, $J = 9.2$ Hz, 1H, Flu), 7.44 (d, $J = 9.2$ Hz, 1H, Flu), 7.18 (t, $J = 6.7$ Hz, 2H, Flu), 6.92 (d, $J = 6.7$ Hz, 1H, Flu), 6.68 (m, 2H, Flu), 6.52 (m, 1H, C_5H_4), 5.40 (m, 1H, C_5H_4), 5.34 (m, 1H, C_5H_4), 4.75 (m, 1H, C_5H_4), 1.56 (s, 3H, CMe_2), 1.48 (s, 3H, CMe_2), −0.24 (s, 9H, $SiMe_3$), −0.59 (s, br, 3H, μ-Me), −1.03 (d, $^2J = 12$ Hz, 1H, $ZrCH_2$), −2.14 (d, $^2J = 12$ Hz, 1H, $ZrCH_2$). ^{13}C NMR (75.47 MHz, 25 °C, toluene-d_8): δ 130.1, 129.3, 126.4, 126.0, 125.7, 125.3, 124.5, 123.3, 122.6, 122.2, 115.4 (Flu), 112.7, 112.0, 104.8, 102.0, 78.5 (C_5H_4), 64.9 ($ZrCH_2$), 39.9 (CMe_2), 27.8, 27.6 (CMe_2), 1.9 ($SiMe_3$).

Preparation of (IPCF)Hf(CH_2SiMe_3)(μ-Me)B(C_6F_5)$_3$ (10). By the procedure described for **9**, the compound was generated in the NMR tube from **8** (11 mg, 0.020 mmol) and $B(C_6F_5)_3$ (10 mg, 0.020 mmol). ^1H NMR (300 MHz, 25 °C, toluene-d_8): δ 7.61 (d, $J = 7.5$ Hz, 1H, Flu), 7.41 (d, $J = 7.5$ Hz, 1H, Flu), 7.19 (m, 2H, Flu), 6.98 (d, $J = 8.3$ Hz, 1H, Flu), 6.68 (t, $J = 7.2$ Hz, 1H, Flu), 6.58 (t, $J = 7.77$ Hz, 1H, Flu), 6.48 (m, 1H, C_5H_4), 5.37 (m, 1H, C_5H_4), 5.09 (m, 1H, C_5H_4), 4.65 (m, 1H, C_5H_4), 1.62 (s, 3H, CMe_2), 1.50 (s, 3H, CMe_2), −0.21 (s, 9H, $SiMe_3$), −0.44 (s, bs, 3H, μ-Me), −2.75 (d, $^2J = 12$ Hz, 1H, $HfCH_2$), −1.37 (d, $^2J = 12$ Hz, 1H, $HfCH_2$). ^{13}C NMR (75.47 MHz, 25 °C, toluene-d_8): δ 129.5, 125.8, 125.6, 125.1, 124.1, 122.9, 122.8, 122.3, 121.7, 121.4, 111.3 (Flu), 115.3, 115.2, 102.6, 100.1, 79.1 (C_5H_4), 56.9 ($HfCH_2$), 40.5 (CMe_2), 28.0, 27.8 (CMe_2), 2.3 ($SiMe_3$).

Preparation of [(IPCF)Zr(CH_2SiMe_3)$^+$···B(C_6F_5)$_4^-$] (11). Complex **7** (9 mg, 0.020 mmol) and $[CPh_3][B(C_6F_5)_4]$ (18 mg, 0.020 mmol) were loaded as solids into a 5 mm NMR tube and dissolved in 1 mL of toluene-d_8 containing 10 vol % of dry 1,2-difluorobenzene to ensure a homogeneous solution. Solutions of **11** in this solvent mixture were thermally stable at room temperature for extended periods of time. ^1H NMR (300 MHz, 10 °C, 9:1 v:v toluene-d_8−$F_2C_6H_4$): δ 7.5−6.3 (Flu, overlapping with toluene, $F_2C_6H_4$, and byproduct Ph_3CMe), 5.99 (m, 1H, C_5H_4), 5.10 (d, 1H, C_5H_4), 5.05 (m, 1H, C_5H_4), 4.63 (m, 1H, C_5H_4), 1.98 (s, 3H, CMe_2), 1.82 (s, 3H, CMe_2), 1.62 (d, $^2J = 12$ Hz, 1H, $ZrCH_2$), −0.71 (s, 9H, $SiMe_3$), −1.21 (d, $^2J = 12$ Hz, 1H, $ZrCH_2$). ^{13}C NMR (75.47 MHz, 10 °C, toluene-d_8): δ 150−115 (Flu, overlapped with toluene, $F_2C_6H_4$, and byproduct Ph_3CMe), 126.6, 113.1, 106.0, 101.4, 62.1 (C_5H_4), 75.8 ($ZrCH_2$), 52.9 (Ph_3CMe), 40.8 (CMe_2), 30.6 (Ph_3CMe), 27.5 (CMe_2), −0.1 ($SiMe_3$).

Preparation of [(IPCF)Hf(CH_2SiMe_3)$^+$···B(C_6F_5)$_4^-$] (12). Compound **12** was generated in the NMR tube by following the procedure described for **11**, using **8** (11 mg, 0.020 mmol) and $[CPh_3][B(C_6F_5)_4]$ (18 mg, 0.020 mmol). ^1H NMR (300 MHz, 10 °C, 9:1 v:v toluene-d_8−$F_2C_6H_4$): δ 7.5−6.1 (Flu, overlapped with toluene, $F_2C_6H_4$, and byproduct Ph_3CMe), 5.92 (m, 1H, C_5H_4), 5.03 (d, 1H, C_5H_4), 5.02 (m, 1H, C_5H_4), 4.56 (m, 1H, C_5H_4), 1.80 (s, 3H, CMe_2), 1.66 (s, 3H, CMe_2), 1.41 (d, $^2J = 12$ Hz, 1H, $HfCH_2$), −0.64 (s, 9H,

$SiMe_3$), −1.12 (d, ^2J = 12 Hz, 1H, $HfCH_2$). ^{13}C NMR (75.47 MHz, 10 °C, toluene-d_8): δ 150−115 (Flu, overlapping with toluene, $F_2C_6H_4$, and byproduct Ph_3CMe), 125.4, 112.1, 104.2, 99.8, 58.8 (C_5H_4), 74.2 ($ZrCH_2$), 52.9 (Ph_3CMe), 41.2 (CMe_2), 30.6 (Ph_3CMe), 27.6, 27.6 (CMe_2), −0.1 ($SiMe_3$).

HOESY Measurements. Two-dimensional fluorine-detected $^{19}F-^1H$ HOESY or proton-detected $^1H-^{19}F$ HOESY NMR experiments were acquired using the standard four-pulse sequence or the modified version.[36] The number of transients and the number of data points were chosen according to the sample concentration and the desired final digital resolution. Semiquantitative spectra were acquired using a 1 s relaxation delay and 500 ms mixing time.

PGSE Measurements. All the PGSE NMR measurements carried out for this work (Table 3, entries 4, 5, and 9) were performed on a Bruker Avance DRX 400 spectrometer equipped with a direct QNP probe and a *z*-gradient coil controlled by a Great 1/10 gradient unit, by using the standard double stimulated echo pulse sequence[37] at the desired temperature without spinning. The shape of the gradients was rectangular, their duration (δ) was 4 ms, and their strength (G) was varied during the experiments. ^1H PGSE NMR spectra were acquired using 32k points, 16 or 32 scans depending on concentrations, and a spectral width of 5000 Hz. All the spectra were processed with a line broadening of 1.0 Hz (^1H) and 3 Hz (^{19}F). The semilogarithmic plots of $\ln(I/I_0)$ vs G^2 were fitted using a standard linear regression algorithm, giving an R factor always better than 0.99. Gradients were calibrated using the diffusion of HDO in D_2O.[38] Data analysis was carried out according to a literature procedure[39] using the resonances of 1,2-$F_2C_6H_4$, as internal standard.

From the measured self-diffusion coefficients (D_t), the average hydrodynamic radius (r_H) of the diffusing particles were derived by taking advantage of the Stokes−Einstein equation, $D_t = kT/(c\pi\eta r_H)$,[39] where k is the Boltzman constant, T is the temperature, c is a numerical factor, and η is the solution viscosity. From r_H, the average hydrodynamic volumes (V_H) of the aggregates were obtained in the assumption that they have a spherical shape. The aggregation number (N) was determined by the ratio between V_H and the hydrodynamic volume of a single ion pair (V_H^{IPO}). V_H^{IPO} was estimated as the sum of the hydrodynamic volumes of the separated ions (V_H^{0+} and V_H^{0-}).[40] V_H^{0+} of $[(IPCF)Zr(CH_2SiMe_3)]+$ was considered equal to 416 Å^3: i.e., the experimental value of 438 Å^3 measured for the corresponding neutral precursor minus the van der Waals volume of a Me group (22 Å^3). It was assumed that the $[(SBI)Zr(CH_2SiMe_3)]^+$ cation has the same volume. V_H^{0-} of $[B(C_6F_5)_4]^-$ (550 Å^3) was estimated by scaling its van der Waals volume (V_{VdW}) for the same factor (V_H^{0-}/V_{VdW}) observed for the $[B(C_6H_5)_4]^-$ anion (432 Å^3) having the same shape.[28] Consequently, the V_H^{IPO} values were 966 Å^3 for both **11** and **13**.

X-ray Crystallography. In all cases, crystals were suspended in perfluorinated polyether oil, mounted on a glass fiber, and transferred directly to the cold N_2 stream of either a Nonius KappaCCD diffractometer (**1**) or an Oxford Diffraction Xcalibur-3 diffractometer (**4** and **5**), in both cases equipped with molybdenum targets (λ(Mo Kα) = 0.710 69 Å). Data collection and processing were carried out using either DENZO and SCALEPACK[41] (**1**) or Oxford Diffraction CrysAlis CCD and RED programs[42] (**4** and **5**). Structure solutions were carried out by direct methods using SHELXS[43] (**1**) and SIR92[44] (**4**) or by heavy-atom methods in DIRDIF-99[45] (**5**). In all cases refinement was carried out by full-matrix least-squares methods using SHELXL-97[43] within the WinGX program suite.[46] Non-hydrogen atoms were refined with anisotropic thermal parameters. Hydrogen atoms were included using a riding model. Crystal and refinement data are collected in Table 5.

Table 5. Crystal Data and Refinement Details

	(IPCF)Zr(CH_2SiMe_3)$_2$ (**1**)	(IPCF)$HfMe_2$ (**4**)	(IPCF)ZrMeCl (**5**)
formula	$C_{29}H_{40}Si_2Zr$	$C_{23}H_{24}Hf$	$C_{22}H_{21}ClZr$
formula wt	536.0	478.9	412.1
cryst syst	orthorhombic	monoclinic	monoclinic
space group	*Pccn* (No. 56)	$P2_1/c$ (No. 14)	$P2_1/c$ (No. 14)
a/Å	37.3040(9)	9.3987(9)	9.2398(6)
b/Å	16.6904(3)	10.7366(10)	10.7676(6)
c/Å	8.9689(2)	18.2206(15)	18.156(3)
β/deg	90	102.011(7)	102.353(11)
V/Å^3	5584.2(2)	1798.4(3)	1764.5(3)
Z	8	4	4
T/K	180(1)	180(2)	140(2)
μ/mm^{-1}	0.494	5.80	0.774
no. of data collected	14 413	24 638	13 612
no. of unique data	3415	4114	13 635
R_{int}	0.095	0.046	n/a
no. of obsd data	2160	3402	9290
R1 ($I > 2\sigma(I)$ and all data)	0.064, 0.119	0.058, 0.068	0.098, 0.127
wR2 (all data)	0.112	0.133	0.293

Compound **5** was found to be nonmerohedrally twinned, and therefore refinement was carried out against an HKLF5 reflection file with four components. Residual unassigned twin components resulted in a residual electron density of a maximum of 3.283 e Å^{-3} approximately equidistant between C(20) and C(21). The methyl group and chloride attached to zirconium were disordered over the two possible positions, with an occupancy of 0.673(8) for the isomer, as shown in Figure 3.

Acknowledgment. This work was supported by the Engineering and Physical Sciences Research Council. C.A.-M. acknowledges financial support from the Junta de Comunidades de Castilla-La Mancha and the Fondo Social Europeo (Grant No. 05/24). We thank Dr. F. Song (SA-Hightech) for helpful discussions and are grateful to Dr. J. E. Davies of the Department of Chemistry, University of Cambridge, for the measurement and processing of the diffraction intensities of complex **1**.

Supporting Information Available: Text and tables giving computational details for QM and MD calculations and crystal and refinement data for compounds **1**, **4**, and **5**. Crystal data are also given as CIF files. This material is available free of charge via the Internet at http://pubs.acs.org.

OM800486P

(36) Lix, B.; Sönnichsen, F. D.; Sykes, B. D. *J. Magn. Reson. A* **1996**, *121*, 83.

(37) (a) Jerschow, A.; Mueller, N. *J. Magn. Reson. A* **1996**, *123*, 222. (b) Jerschow, A.; Mueller, N. *J. Magn. Reson. A* **1997**, *125*, 372. (c) Valentini, M.; Rüegger, H.; Pregosin, P. S *Helv. Chim. Acta* **2001**, *84*, 2833, and references therein.

(38) Mills, R. *J. Phys. Chem.* **1973**, *77*, 685.

(39) Macchioni, A.; Ciancaleoni, G.; Zuccaccia, C.; Zuccaccia, D. *Chem. Soc. Rev.* **2008**, *37*, 479.

(40) Ciancaleoni, G.; Zuccaccia, C.; Zuccaccia, D.; Macchioni, A. *Organometallics* **2007**, *26*, 3624.

(41) Otwinowski, Z.; Minor, W. In *Macromolecular Crystallography, Part A*; Carter, C. W., Jr., Sweet, R. M., Eds.; Academic Press: New York, 1997; Methods in Enzymology Vol. *276*, pp 307−326.

(42) Oxford Diffraction ABSPACK, CrysAlis CCD, and CrysAlis RED, Versions 1.171; Oxford Diffraction Ltd., Abingdon, Oxford, England, 2005.

(43) Sheldrick, G. M. SHELX-97: Programs for Crystal Structure Determination (SHELXS) and Refinement (SHELXL); University of Göttingen, Göttingen, Germany, 1997.

(44) Altomare, A.; Cascarano, G.; Giacovazzo, C.; Guagliardi, A. *J. Appl. Crystallogr.* **1993**, *26*, 343–350.

(45) Beurskens, P. T.; Beurskens, G.; de Gelder, R.; Garcia-Granda, S.; Israel, R.; Gould, R. O.; Smits, J. M. M. The DIRDIF-99 Program System; Crystallography Laboratory, University of Nijmegen, Nijmegen, The Netherlands. 1999.

(46) Farrugia, L. J. *J. Appl. Crystallogr.* **1999**, *32*, 837.